SUPPLEMENTARY INFORMATION FOR THE PAPER

The *ab initio* potential energy curves of atom pairs and transport properties of high-temperature vapors of Cu and Si and their mixtures with He, Ar, and Xe gases

Kevin W. Kayang,[1] Alexey N. Volkov,[1,*] Petr A. Zhilyaev,[2] and Felix Sharipov[3]

1 - Department of Mechanical Engineering, University of Alabama, 7th Avenue, Tuscaloosa, AL 35487, USA

2 - Center for Materials Technologies, Skolkovo Institute of Science and Technology, 121205, Bolshoy Boulevard 30, bld. 1, Moscow, Russia

3 - Departamento de Física, Universidade Federal do Paraná, Caixa Postal 19044, Curitiba 81531-980, Brazil

* - Corresponding author, e-mail: avolkov1@ua.edu

This Supplementary material includes the discussion of the choice of numerical parameters for the quantum Monte Carlo (QMC) calculations (Section S1), tables with the atom pair (dimer) energies obtained in the QMC calculations (Section S2), description of the approach used to parameterize the Morse long range (MLR) potential (Section S3), comparison of the QMC potential energy curves (PECs) with available literature data (Section S4), additional plots that characterize the effect of the PEC shape on the scattering of atoms in binary collisions (Section S5), discussion of the choice of the numerical parameters used for calculation of the transport coefficients (Section S6), plots of the major transport collision integrals for various atom pairs and viscosity of noble gases (Section S7), plots that characterize the effect of the LJ and VSS approximations on the transport coefficients of the Cu-Ar mixture (Section S8), and description of additional supplementary files containing the tabulated transport coefficients (Section S9).

S1. Convergence study of the QMC calculations

In all QMC calculations, the optimization of the wave function was performed using the adaptive linear method to improve the accuracy and efficiency of computations. The QMC adaptive linear method works iteratively by first setting up the Hamiltonian of the linear optimization method[S1] with overlapped matrices and different shifts. Then the eigenvalue problem

is solved for each shift and the wave function is updated. The updated wave function corresponding to the best cost function is then selected.

A preliminary parametric study was performed to validate the convergence of the QMC calculations of the dimer energies with respect to all primary numerical parameters of the QMCPACK package.[S2] The selected results of this study for the He-He and He-Cu dimers are presented in Fig. S1 and S2. The dimers that include He atoms are chosen to present the results of the convergence study since the corresponding dimers have the smallest potential well depths D_e. This puts the most severe restrictions on the values of numerical parameters. For other dimers, further computations showed that the convergence of energy is ensured at the same or less restrictive values of the numerical parameters.

The results of the test computations are shown in Fig. S1 and S2 in terms of the relative energy difference $\Delta[E]$ as a function of some parameter P

$$\Delta[E](P) = \left|\frac{E(P) - E(P_{\mathrm{ref}})}{E(P_{\mathrm{ref}})}\right|, \tag{S1}$$

where $E(P)$ is the dimer energy when the parameter is equal to P and P_{ref} is the maximum value of the parameter, which presumably corresponds to numerical convergence. For each parameter, a series of simulations with sequentially doubling values of the parameters ($P_{n+1} = 2P_n$) was performed until the difference $|[E(P_{n+1}) - E(P_n)]/E(P_{n+1})|$ for the two last values of energy in the sequence becomes smaller than $10^{-4} - 10^{-5}$. Then the last value of the parameter in the sequence was considered as P_{ref}.

Fig. S1 displays the relative energy difference for the He-He dimer at $r = 2.96$ Å $\approx r_{\mathrm{e}}$ (here r is the interatomic distance and r_{e} is the equilibrium interatomic distance) as a function of the number of statistical samples N_S, which determines the statistical error of the QMC method. The number of samples here is varied from 800 to 102400. In this case, convergence is achieved if the number of samples is equal to or greater than 51200. This relatively large number of samples is required to obtain an agreement with the coupled cluster singles and doubles with perturbative triples corrections [CCSD(T)] calculations of energy for the He-He dimer.[S3] The results of the QMC calculations of energy for the V-He dimers (V=Cu or Si) are also found to be very sensitive to the number of samples. The QMC calculations for other dimers considered in the present work can be performed with somewhat smaller N_S.

Once the number of samples, which is required to ensure that the magnitude of the statistical error is sufficiently small, was determined, the values of other numerical parameters that allow one to reduce the magnitude of the systematic error to a required level were chosen next at fixed N_S. The systematic error of calculations with the QMCPACK package is determined primarily by the number of optimization cycles N_O of the variational Monte Carlo (VMC) scheme, time step Δt of the diffusion Monte Carlo (DMC) calculations, and number of random walkers N_W. In Fig. S2, the results of the convergence study with respect to these parameters obtained for the He-He and Cu-He dimers at $r = 2.96$ Å and $r = 4.6$ Å, respectively, are presented.

First, the number of optimization cycles needed to obtain a converged VMC energy was determined. Fig. S2(a) shows the relative energy difference as a function of the optimization cycle number. In the cases of the He-He and Cu-He dimers, the trial wave functions obtained from the DFT calculations were of good accuracy since a high wave function cutoff was used in addition to the pseudopotentials specifically developed for the QMC calculations. A relative energy difference of 10^{-4} was chosen as the convergence threshold. Then the convergence is achieved after the third optimization step for the He-He dimer and after the first optimization step for the Cu-He dimer. The convergence can be achieved after more optimization cycles if the trial wave function is not accurate, so the number of the optimization cycles was chosen to be equal to 9 for all subsequent calculations.

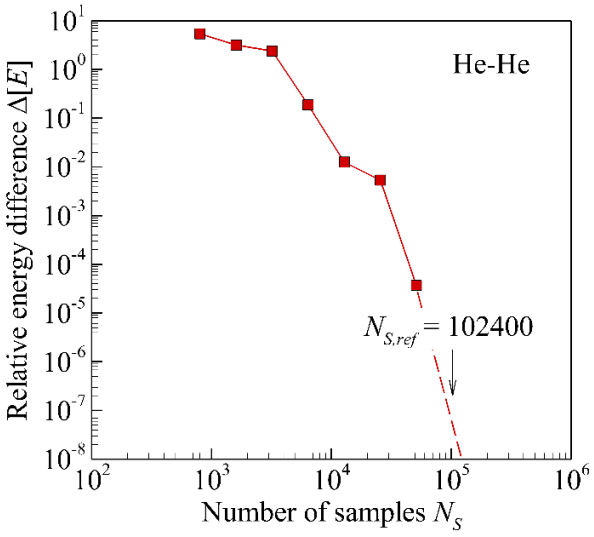

Fig. S1 Relative differences of energy $\Delta[E]$, enq (S1), *versus* number of samples N_S for the He-He dimer at $r = 2.96$ Å. The reference value of energy in eqn (S1) corresponds to $N_S = 102400$. The symbols correspond to the calculated values, while the curves are drawn only to guide the eye.

Next, the effect of the time step Δt in the DMC calculations was analyzed. The output from the VMC calculations was fed into the DMC input, and the time step was varied from 0.1 a.u. to 0.005 a.u.. The relative difference between the DMC energy *versus* the inverse time step is shown in Fig. S2(b). The results indicate a practically linear decrease in $\Delta[E]$ with increasing Δt^{-1}. With a convergence threshold of 10^{-4}, the energy of the Cu-He dimer is already converged with the largest time step, whereas the energy of the He-He dimer converges at $\Delta t = 0.01$ a.u. The time step of 0.005 a.u. is therefore chosen for all subsequent calculations.

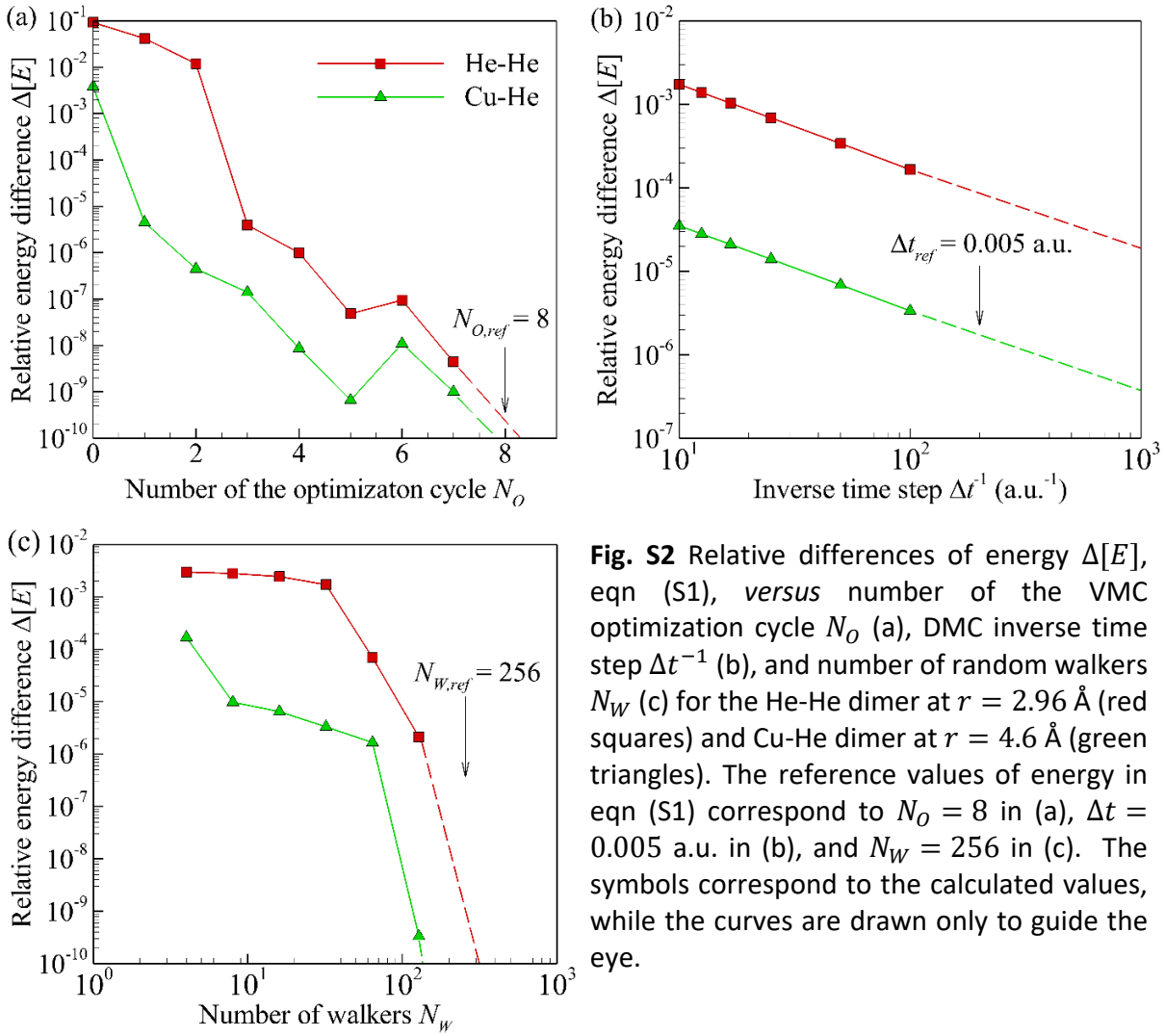

Fig. S2 Relative differences of energy $\Delta[E]$, eqn (S1), *versus* number of the VMC optimization cycle N_O (a), DMC inverse time step Δt^{-1} (b), and number of random walkers N_W (c) for the He-He dimer at $r = 2.96$ Å (red squares) and Cu-He dimer at $r = 4.6$ Å (green triangles). The reference values of energy in eqn (S1) correspond to $N_O = 8$ in (a), $\Delta t = 0.005$ a.u. in (b), and $N_W = 256$ in (c). The symbols correspond to the calculated values, while the curves are drawn only to guide the eye.

Finally, a study of the effect of the random walker number N_W is performed for the preliminary chosen N_S, N_O, and Δt. The number of walkers needed depends on the complexity of the system and the accuracy of initial approximation of the wave function obtained in the VMC

calculations. The values of $\Delta[E]$ *versus* N_W shown in Fig. S2(c) indicate that the convergence occurs at $N_W = 64$ for the Cu-He dimer and at $N_W = 128$ for the He-He dimer. It is worth noting that a further increase in N_W may not significantly increase the accuracy of the QMC calculations.[S2]

Based on the results of the convergence study, all further QMC calculations were performed with the number of statistical samples ranging from 12800 to 51200. The number of the VMC optimization cycle was equal to 9. The DMC calculations were performed using 128 to 256 random walkers, with the DMC walkers being initialized from the VMC random walk, with a time step of 0.005 a.u.

S2. Tabulated energies of dimers found in the QMC calculations

The values of energy found in the QMC calculations performed in the present work are presented in Table S1 for the homonuclear He-He, Ar-Ar, Cu-Cu, and Si-Si dimers, in Table S2 for the heteronuclear Cu-He, Cu-Ar, and Cu-He dimers, and in Table S3 for the heteronuclear Si-He, Si-Ar, and Si-Xe dimers. As a rule, the calculations were first performed with the increment of the interatomic distance $\Delta r = 0.5$ Å from $r = 10$ Å to $r = 6$ Å and with $\Delta r = 0.1$ Å from $r = 6$ Å to a distance r_{mm} that corresponds to strong repulsion with $V(r_{\mathrm{mm}})\sim 10^2 - 10^3$ eV. Then the approximate position of the energy minimum was identified, and the additional values of energy were calculated in the vicinity of the $r = r_{\mathrm{e}}$ with an increment of $\Delta r = 0.02$ Å.

S3. Parametrization of the Morse long range (MLR) potentials

For each dimer, the parameters of the MLR potential were determined by multifactorial non-linear least-square fitting that minimizes the relative root-mean-square (RMS) deviation, eqn (6), in a range of interatomic distances $r_{\mathrm{f,min}} \le r \le r_{\mathrm{f,max}}$. The boundaries of this range (Table S4) are chosen individually for each dimer to ensure that the MLR potential has only one extremum at $r = r_e$ and $r_{\mathrm{f,min}}$ is small enough to enable accurate calculations of the transport coefficients of corresponding gases or gaseous mixtures at temperatures $T \le T_{\mathrm{max}} = 10^4$ K

The local relative difference $\Delta_i = \left[V(r_i) - V_{\mathrm{QMC}(i)}\right]/V_{\mathrm{QMC}(i)}$, between the MLR potential $V(r_i)$ at $r = r_i$ and corresponding QMC data point $V_{\mathrm{QMC}(i)}$ in the ranges $r_{f,min} \le r \le r_{f,max}$ are shown in Fig. S3 for the homonuclear Cu-Cu and Si-Si dimers as well as for all considered

heteronuclear dimers. With exception of a few outliers, the absolute values of Δ_i are less than 0.05. The values of the relative RMS deviation for most dimers span the range from ~0.005 to ~0.03 but approach 0.05 for the Ar-Ar and Cu-Cu dimers (Table S4). The calculated values of Δ_i and RMS deviation indicate that the obtained fits in the form of the MLR potentials provide a uniformly accurate approximation of the QMC data points down to distances where $V(r) > \sim 50$ eV, *cf.* values of $V_{\mathrm{f,min}} = V(r_{\mathrm{f,min}})$ in Table S4, with exception of the He-He and Cu-Ar dimers, where $V_{f,min} \sim 20$ eV.

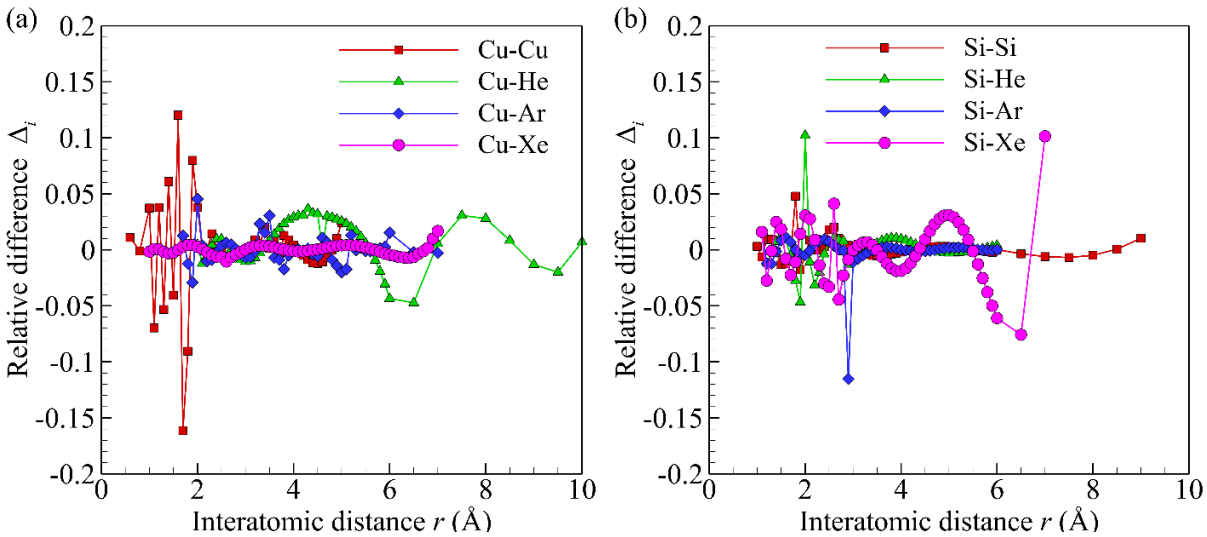

Fig. S3 Relative difference Δ_i between the potential energy obtained in the QMC calculations and MLR potentials for dimers involving Cu (a) and Si (b) atoms. The symbols represent the calculated values, while the curves are drawn only to guide the eye.

The parametric study of the effects of the numerical parameters on the accuracy of the calculation of the transport coefficients (Section S6) showed that the maximum relative velocity C_r of two atoms in a binary collision, which defines the top integration limit in the numerical calculations of the transport collision integrals in eqn (14), must correspond to an equivalent temperature T_{**} that is about ten times greater than T_{max}. The values of the relative velocity C_{**} and corresponding minimum interatomic distance r_{**} realized at head-to-head collisions calculated for $T_{**} = 10^5$ K from the equation $3k_B T_{**}/2 = mC_{r**}^2/2 = V(r_{**}) = 12.93$ eV (m is the reduced mass of colliding atoms, $V(r)$ is calculated by piecewise-liner interpolation between the QMC data points) are shown in Table S4. It is clear that r_{**} are significantly greater than $r_{\mathrm{f,min}}$ for all dimers with exception of the Cu-Ar dimer, where r_{**} is only 4% larger than $r_{f,min}$.

Table S1 Energy (eV) of the homonuclear He-He, Ar-Ar, Cu-Cu, and Si-Si dimers *versus* interatomic distance r (Å) found in the QMC calculations.

Distance	Dimer			
r (Å)	He-He	Ar-Ar	Cu-Cu	Si-Si
0.2	$1.026 \cdot 10^{2}$	-	-	-
0.4	$3.988 \cdot 10^{1}$	-	-	-
0.6	$1.889 \cdot 10^{1}$	$4.704 \cdot 10^{2}$	$5.145 \cdot 10^{2}$	$1.762 \cdot 10^{2}$
0.8	8.753	$2.153 \cdot 10^{2}$	$1.952 \cdot 10^{2}$	$9.114 \cdot 10^{1}$
1	3.942	-	$7.653 \cdot 10^{1}$	$4.718 \cdot 10^{1}$
1.1	2.620	$6.602 \cdot 10^{1}$	$5.329 \cdot 10^{1}$	$3.322 \cdot 10^{1}$
1.2	1.730	$4.765 \cdot 10^{1}$	$3.005 \cdot 10^{1}$	$2.262 \cdot 10^{1}$
1.3	1.135	$3.790 \cdot 10^{1}$	$2.067 \cdot 10^{1}$	$1.464 \cdot 10^{1}$
1.4	$7.390 \cdot 10^{-1}$	$2.789 \cdot 10^{1}$	$1.128 \cdot 10^{1}$	8.777
1.5	$4.778 \cdot 10^{-1}$	$2.148 \cdot 10^{1}$	7.157	4.594
1.6	$3.064 \cdot 10^{-1}$	$1.587 \cdot 10^{1}$	3.029	1.718
1.7	$1.947 \cdot 10^{-1}$	$1.157 \cdot 10^{1}$	1.256	$-1.663 \cdot 10^{-1}$
1.8	$1.223 \cdot 10^{-1}$	8.270	$-5.171 \cdot 10^{-1}$	-1.320
1.9	$7.583 \cdot 10^{-2}$	6.259	-1.298	-2.226
2	$4.621 \cdot 10^{-2}$	4.296	-1.845	-
2.1	$2.752 \cdot 10^{-2}$	2.917	-2.141	-3.020
2.2	$1.587 \cdot 10^{-2}$	2.107	-2.199	-3.218
2.3	$8.700 \cdot 10^{-3}$	1.599	-2.118	-3.254
2.4	$4.376 \cdot 10^{-3}$	1.210	-2.038	-3.163
2.5	$1.828 \cdot 10^{-3}$	$8.345 \cdot 10^{-1}$	-1.902	-2.941
2.6	$3.802 \cdot 10^{-4}$	$4.870 \cdot 10^{-1}$	-1.767	-2.696
2.7	$-3.986 \cdot 10^{-4}$	$3.399 \cdot 10^{-1}$	-1.606	-2.441
2.8	$-7.779 \cdot 10^{-4}$	$2.083 \cdot 10^{-1}$	-1.446	-2.170
2.9	$-9.251 \cdot 10^{-4}$	$1.395 \cdot 10^{-1}$	-1.295	-1.871
2.96	$-9.466 \cdot 10^{-4}$	-	-	-
3	$-9.427 \cdot 10^{-4}$	$7.772 \cdot 10^{-2}$	-1.145	-1.611
3.1	$-8.926 \cdot 10^{-4}$	$4.169 \cdot 10^{-2}$	$-9.937 \cdot 10^{-1}$	-1.359
3.2	$-8.112 \cdot 10^{-4}$	$1.999 \cdot 10^{-2}$	$-8.422 \cdot 10^{-1}$	-1.156
3.3	$-7.191 \cdot 10^{-4}$	$5.085 \cdot 10^{-3}$	$-7.176 \cdot 10^{-1}$	$-9.747 \cdot 10^{-1}$
3.4	$-6.278 \cdot 10^{-4}$	$-3.350 \cdot 10^{-3}$	$-5.929 \cdot 10^{-1}$	$-8.198 \cdot 10^{-1}$
3.42	-	$-4.332 \cdot 10^{-3}$	-	-
3.44	-	$-5.804 \cdot 10^{-3}$	-	-
3.46	-	$-6.786 \cdot 10^{-3}$	-	-
3.48	-	$-7.768 \cdot 10^{-3}$	-	-
3.5	$-5.429 \cdot 10^{-4}$	$-8.588 \cdot 10^{-3}$	$-5.004 \cdot 10^{-1}$	$-6.891 \cdot 10^{-1}$
3.52	-	$-9.097 \cdot 10^{-3}$	-	-
3.54	-	$-9.606 \cdot 10^{-3}$	-	-

Table S1. Continued.

Distance	Dimer			
r (Å)	He-He	Ar-Ar	Cu-Cu	Si-Si
3.56	-	$-1.012\cdot10^{-2}$	-	-
3.58	-	$-1.063\cdot10^{-2}$	-	-
3.6	$-4.669\cdot10^{-4}$	$-1.111\cdot10^{-2}$	$-4.078\cdot10^{-1}$	$-5.795\cdot10^{-1}$
3.7	$-4.004\cdot10^{-4}$	$-1.217\cdot10^{-2}$	$-3.361\cdot10^{-1}$	$-4.880\cdot10^{-1}$
3.8	$-3.430\cdot10^{-4}$	$-1.223\cdot10^{-2}$	$-2.657\cdot10^{-1}$	$-4.118\cdot10^{-1}$
3.9	$-2.940\cdot10^{-4}$	$-1.197\cdot10^{-2}$	$-2.138\cdot10^{-1}$	$-3.483\cdot10^{-1}$
4	$-2.522\cdot10^{-4}$	$-1.100\cdot10^{-2}$	$-1.713\cdot10^{-1}$	$-2.954\cdot10^{-1}$
4.1	$-2.168\cdot10^{-4}$	$-1.001\cdot10^{-2}$	$-1.369\cdot10^{-1}$	$-2.513\cdot10^{-1}$
4.2	$-1.868\cdot10^{-4}$	$-8.966\cdot10^{-3}$	$-1.092\cdot10^{-1}$	$-2.145\cdot10^{-1}$
4.3	$-1.614\cdot10^{-4}$	$-8.062\cdot10^{-3}$	$-8.691\cdot10^{-2}$	$-1.837\cdot10^{-1}$
4.4	$-1.399\cdot10^{-4}$	$-7.164\cdot10^{-3}$	$-6.914\cdot10^{-2}$	$-1.579\cdot10^{-1}$
4.5	$-1.215\cdot10^{-4}$	$-6.287\cdot10^{-3}$	$-5.499\cdot10^{-2}$	$-1.361\cdot10^{-1}$
4.6	$-1.059\cdot10^{-4}$	$-5.581\cdot10^{-3}$	$-4.373\cdot10^{-2}$	$-1.177\cdot10^{-1}$
4.7	$-9.256\cdot10^{-5}$	$-4.871\cdot10^{-3}$	$-3.479\cdot10^{-2}$	$-1.021\cdot10^{-1}$
4.8	$-8.113\cdot10^{-5}$	$-4.273\cdot10^{-3}$	$-2.768\cdot10^{-2}$	$-8.892\cdot10^{-2}$
4.9	$-7.131\cdot10^{-5}$	$-3.745\cdot10^{-3}$	$-2.204\cdot10^{-2}$	$-7.765\cdot10^{-2}$
5	$-6.285\cdot10^{-5}$	$-3.276\cdot10^{-3}$	$-1.756\cdot10^{-2}$	$-6.801\cdot10^{-2}$
5.1	$-5.554\cdot10^{-5}$	-	$-1.399\cdot10^{-2}$	$-5.974\cdot10^{-2}$
5.2	$-4.920\cdot10^{-5}$	$-2.578\cdot10^{-3}$	$-1.115\cdot10^{-2}$	$-5.262\cdot10^{-2}$
5.3	$-4.370\cdot10^{-5}$	-	$-8.886\cdot10^{-3}$	$-4.648\cdot10^{-2}$
5.4	$-3.890\cdot10^{-5}$	$-2.020\cdot10^{-3}$	$-7.079\cdot10^{-3}$	$-4.117\cdot10^{-2}$
5.5	$-3.471\cdot10^{-5}$	-	$-5.635\cdot10^{-3}$	$-3.655\cdot10^{-2}$
5.6	$-3.104\cdot10^{-5}$	$-1.596\cdot10^{-3}$	$-4.478\cdot10^{-3}$	$-3.253\cdot10^{-2}$
5.7	$-2.781\cdot10^{-5}$	-	$-3.552\cdot10^{-3}$	$-2.902\cdot10^{-2}$
5.8	$-2.497\cdot10^{-5}$	$-1.287\cdot10^{-3}$	$-2.809\cdot10^{-3}$	$-2.595\cdot10^{-2}$
5.9	$-2.247\cdot10^{-5}$	-	$-2.212\cdot10^{-3}$	$-2.325\cdot10^{-2}$
6	$-2.025\cdot10^{-5}$	$-1.032\cdot10^{-3}$	$-1.733\cdot10^{-3}$	$-2.082\cdot10^{-2}$
6.5	$-1.237\cdot10^{-5}$	$-5.080\cdot10^{-4}$	$-9.984\cdot10^{-4}$	$-1.252\cdot10^{-2}$
7	$-7.853\cdot10^{-6}$	$-2.940\cdot10^{-4}$	$-7.091\cdot10^{-4}$	$-7.854\cdot10^{-3}$
7.5	$-5.150\cdot10^{-6}$	$-1.200\cdot10^{-4}$	$-5.398\cdot10^{-4}$	$-5.109\cdot10^{-3}$
8	$-3.475\cdot10^{-6}$	$-9.425\cdot10^{-5}$	$-3.075\cdot10^{-4}$	$-3.426\cdot10^{-3}$
8.5	$-2.403\cdot10^{-6}$	$-5.600\cdot10^{-5}$	$-2.264\cdot10^{-4}$	$-2.359\cdot10^{-3}$
9	$-1.698\cdot10^{-6}$	-	$-1.759\cdot10^{-4}$	$-1.662\cdot10^{-3}$
9.5	$-1.223\cdot10^{-6}$	-	$-1.431\cdot10^{-4}$	$-1.195\cdot10^{-3}$
10	$-8.962\cdot10^{-7}$	-	$-1.420\cdot10^{-4}$	$-8.742\cdot10^{-4}$

Table S2 Energy (eV) of the heteronuclear Cu-He, Cu-Ar, and Cu-Xe dimers *versus* interatomic distance r (Å) found in the QMC calculations.

Distance	Dimer		
r (Å)	Cu-He	Cu-Ar	Cu-Xe
1	-	-	$1.471 \cdot 10^{2}$
1.1	-	-	$9.772 \cdot 10^{1}$
1.2	-	-	$6.517 \cdot 10^{1}$
1.3	-	-	$4.365 \cdot 10^{1}$
1.4	-	$4.225 \cdot 10^{2}$	$2.927 \cdot 10^{1}$
1.5	-	$1.336 \cdot 10^{2}$	$1.956 \cdot 10^{1}$
1.6	-	$4.923 \cdot 10^{1}$	$1.298 \cdot 10^{1}$
1.7	-	$2.061 \cdot 10^{1}$	8.514
1.8	-	9.613	5.513
1.9	-	4.911	3.516
2	$2.759 \cdot 10^{3}$	2.509	2.200
2.1	$1.402 \cdot 10^{3}$	1.555	1.342
2.2	$7.246 \cdot 10^{2}$	$9.973 \cdot 10^{-1}$	$7.879 \cdot 10^{-1}$
2.3	$3.791 \cdot 10^{2}$	$6.580 \cdot 10^{-1}$	$4.337 \cdot 10^{-1}$
2.4	$1.999 \cdot 10^{2}$	$4.437 \cdot 10^{-1}$	$2.094 \cdot 10^{-1}$
2.5	$1.059 \cdot 10^{2}$	$3.040 \cdot 10^{-1}$	$6.902 \cdot 10^{-2}$
2.6	$5.618 \cdot 10^{1}$	$2.103 \cdot 10^{-1}$	$-1.731 \cdot 10^{-2}$
2.7	$2.979 \cdot 10^{1}$	$1.460 \cdot 10^{-1}$	$-6.877 \cdot 10^{-2}$
2.8	$1.578 \cdot 10^{1}$	$1.009 \cdot 10^{-1}$	$-9.776 \cdot 10^{-2}$
2.9	8.337	$6.896 \cdot 10^{-2}$	$-1.123 \cdot 10^{-1}$
3	4.396	$4.597 \cdot 10^{-2}$	$-1.175 \cdot 10^{-1}$
3.1	2.314	$2.932 \cdot 10^{-2}$	$-1.169 \cdot 10^{-1}$
3.2	1.217	$1.721 \cdot 10^{-2}$	$-1.127 \cdot 10^{-1}$
3.3	$6.393 \cdot 10^{-1}$	$8.348 \cdot 10^{-3}$	$-1.064 \cdot 10^{-1}$
3.4	$3.358 \cdot 10^{-1}$	$2.238 \cdot 10^{-3}$	$-9.898 \cdot 10^{-2}$
3.5	$1.763 \cdot 10^{-1}$	$-2.174 \cdot 10^{-3}$	$-9.104 \cdot 10^{-2}$
3.6	$9.234 \cdot 10^{-2}$	$-5.470 \cdot 10^{-3}$	$-8.301 \cdot 10^{-2}$
3.7	$4.810 \cdot 10^{-2}$	$-7.677 \cdot 10^{-3}$	$-7.517 \cdot 10^{-2}$
3.8	$2.475 \cdot 10^{-2}$	$-9.160 \cdot 10^{-3}$	$-6.768 \cdot 10^{-2}$
3.9	$1.242 \cdot 10^{-2}$	$-9.833 \cdot 10^{-3}$	$-6.066 \cdot 10^{-2}$
4	$5.909 \cdot 10^{-3}$	$-1.010 \cdot 10^{-2}$	$-5.414 \cdot 10^{-2}$
4.1	$2.498 \cdot 10^{-3}$	$-1.007 \cdot 10^{-2}$	$-4.817 \cdot 10^{-2}$
4.2	$7.341 \cdot 10^{-4}$	$-9.802 \cdot 10^{-3}$	$-4.273 \cdot 10^{-2}$
4.3	$-1.530 \cdot 10^{-4}$	$-9.335 \cdot 10^{-3}$	$-3.781 \cdot 10^{-2}$
4.4	$-5.742 \cdot 10^{-4}$	$-8.828 \cdot 10^{-3}$	$-3.339 \cdot 10^{-2}$
4.5	$-7.501 \cdot 10^{-4}$	$-8.223 \cdot 10^{-3}$	$-2.944 \cdot 10^{-2}$
4.6	$-8.232 \cdot 10^{-4}$	$-7.463 \cdot 10^{-3}$	$-2.593 \cdot 10^{-2}$

Table S2 Continued.

Distance		Dimer	
r (Å)	Cu-He	Cu-Ar	Cu-Xe
4.7	$-7.851\cdot10^{-4}$	$-6.865\cdot10^{-3}$	$-2.281\cdot10^{-2}$
4.8	$-7.418\cdot10^{-4}$	$-6.357\cdot10^{-3}$	$-2.006\cdot10^{-2}$
4.9	$-6.873\cdot10^{-4}$	$-5.805\cdot10^{-3}$	$-1.763\cdot10^{-2}$
5	$-6.308\cdot10^{-4}$	$-5.284\cdot10^{-3}$	$-1.551\cdot10^{-2}$
5.1	$-5.767\cdot10^{-4}$	$-4.756\cdot10^{-3}$	$-1.364\cdot10^{-2}$
5.2	$-5.271\cdot10^{-4}$	$-4.152\cdot10^{-3}$	$-1.200\cdot10^{-2}$
5.3	$-4.825\cdot10^{-4}$	$-3.779\cdot10^{-3}$	$-1.057\cdot10^{-2}$
5.4	$-4.429\cdot10^{-4}$	$-3.379\cdot10^{-3}$	$-9.324\cdot10^{-3}$
5.5	$-4.080\cdot10^{-4}$	$-3.028\cdot10^{-3}$	$-8.233\cdot10^{-3}$
5.6	$-3.772\cdot10^{-4}$	$-2.700\cdot10^{-3}$	$-7.278\cdot10^{-3}$
5.7	$-3.501\cdot10^{-4}$	$-2.395\cdot10^{-3}$	$-6.444\cdot10^{-3}$
5.8	$-3.261\cdot10^{-4}$	$-2.121\cdot10^{-3}$	$-5.714\cdot10^{-3}$
5.9	$-3.049\cdot10^{-4}$	$-1.871\cdot10^{-3}$	$-5.077\cdot10^{-3}$
6	$-2.860\cdot10^{-4}$	$-1.626\cdot10^{-3}$	$-4.518\cdot10^{-3}$
6.5	$-1.981\cdot10^{-4}$	$-8.314\cdot10^{-4}$	$-2.594\cdot10^{-3}$
7	$-1.302\cdot10^{-4}$	$-3.853\cdot10^{-4}$	$-1.557\cdot10^{-3}$
7.5	$-8.737\cdot10^{-5}$	$-1.191\cdot10^{-4}$	$-9.770\cdot10^{-4}$
8	$-5.987\cdot10^{-5}$	-	$-6.468\cdot10^{-4}$
8.5	$-4.186\cdot10^{-5}$	-	$-4.535\cdot10^{-4}$
9	$-2.982\cdot10^{-5}$	-	$-3.418\cdot10^{-4}$
9.5	$-2.162\cdot10^{-5}$	-	$-2.846\cdot10^{-4}$
10	$-1.592\cdot10^{-5}$	-	$-2.679\cdot10^{-4}$

Table S3 Energy (eV) of the heteronuclear Si-He, Si-Ar, and Si-Xe dimers *versus* interatomic distance r (Å) found in the QMC calculations.

Distance		Dimer	
r (Å)	Si-He	Si-Ar	Si-Xe
1	-	$3.582\cdot10^{4}$	$1.252\cdot10^{2}$
1.1	-	$8.442\cdot10^{3}$	$9.289\cdot10^{1}$
1.2	-	$2.313\cdot10^{3}$	$6.782\cdot10^{1}$
1.3	$3.012\cdot10^{2}$	$7.222\cdot10^{2}$	$4.874\cdot10^{1}$
1.4	$8.691\cdot10^{1}$	$2.529\cdot10^{2}$	$3.455\cdot10^{1}$
1.5	$2.651\cdot10^{1}$	$9.812\cdot10^{1}$	$2.420\cdot10^{1}$
1.6	8.516	$4.169\cdot10^{1}$	$1.679\cdot10^{1}$
1.7	2.955	$1.921\cdot10^{1}$	$1.155\cdot10^{1}$
1.8	1.166	9.510	7.865
1.9	$5.484\cdot10^{-1}$	5.011	5.295
2	$2.639\cdot10^{-1}$	2.783	3.510
2.1	$1.878\cdot10^{-1}$	1.614	2.275

Table S3 Continued.

Distance	Dimer		
r (Å)	Si-He	Si-Ar	Si-Xe
2.2	$1.302 \cdot 10^{-1}$	$9.662 \cdot 10^{-1}$	1.424
2.3	$8.752 \cdot 10^{-2}$	$5.902 \cdot 10^{-1}$	$8.423 \cdot 10^{-1}$
2.4	$5.655 \cdot 10^{-2}$	$3.624 \cdot 10^{-1}$	$4.490 \cdot 10^{-1}$
2.5	$3.469 \cdot 10^{-2}$	$2.194 \cdot 10^{-1}$	$1.878 \cdot 10^{-1}$
2.6	$1.968 \cdot 10^{-2}$	$1.270 \cdot 10^{-1}$	$1.925 \cdot 10^{-2}$
2.7	$9.671 \cdot 10^{-3}$	$6.621 \cdot 10^{-2}$	$-8.459 \cdot 10^{-2}$
2.8	$3.208 \cdot 10^{-3}$	$2.587 \cdot 10^{-2}$	$-1.438 \cdot 10^{-1}$
2.9	$-8.200 \cdot 10^{-4}$	$-7.254 \cdot 10^{-4}$	$-1.726 \cdot 10^{-1}$
3	$-3.216 \cdot 10^{-3}$	$-1.783 \cdot 10^{-2}$	$-1.811 \cdot 10^{-1}$
3.1	$-4.542 \cdot 10^{-3}$	$-2.827 \cdot 10^{-2}$	$-1.764 \cdot 10^{-1}$
3.2	$-5.183 \cdot 10^{-3}$	$-3.401 \cdot 10^{-2}$	$-1.635 \cdot 10^{-1}$
3.3	$-5.394 \cdot 10^{-3}$	$-3.646 \cdot 10^{-2}$	$-1.467 \cdot 10^{-1}$
3.4	$-5.340 \cdot 10^{-3}$	$-3.667 \cdot 10^{-2}$	$-1.290 \cdot 10^{-1}$
3.5	$-5.130 \cdot 10^{-3}$	$-3.542 \cdot 10^{-2}$	$-1.123 \cdot 10^{-1}$
3.6	$-4.831 \cdot 10^{-3}$	$-3.328 \cdot 10^{-2}$	$-9.721 \cdot 10^{-2}$
3.7	$-4.486 \cdot 10^{-3}$	$-3.066 \cdot 10^{-2}$	$-8.413 \cdot 10^{-2}$
3.8	$-4.123 \cdot 10^{-3}$	$-2.784 \cdot 10^{-2}$	$-7.298 \cdot 10^{-2}$
3.9	$-3.758 \cdot 10^{-3}$	$-2.502 \cdot 10^{-2}$	$-6.357 \cdot 10^{-2}$
4	$-3.402 \cdot 10^{-3}$	$-2.232 \cdot 10^{-2}$	$-5.567 \cdot 10^{-2}$
4.1	$-3.061 \cdot 10^{-3}$	$-1.980 \cdot 10^{-2}$	$-4.904 \cdot 10^{-2}$
4.2	$-2.740 \cdot 10^{-3}$	$-1.751 \cdot 10^{-2}$	$-4.346 \cdot 10^{-2}$
4.3	$-2.441 \cdot 10^{-3}$	$-1.545 \cdot 10^{-2}$	$-3.874 \cdot 10^{-2}$
4.4	$-2.165 \cdot 10^{-3}$	$-1.361 \cdot 10^{-2}$	$-3.473 \cdot 10^{-2}$
4.5	$-1.913 \cdot 10^{-3}$	$-1.199 \cdot 10^{-2}$	$-3.128 \cdot 10^{-2}$
4.6	$-1.684 \cdot 10^{-3}$	$-1.056 \cdot 10^{-2}$	$-2.830 \cdot 10^{-2}$
4.7	$-1.477 \cdot 10^{-3}$	$-9.306 \cdot 10^{-3}$	$-2.571 \cdot 10^{-2}$
4.8	$-1.292 \cdot 10^{-3}$	$-8.207 \cdot 10^{-3}$	$-2.342 \cdot 10^{-2}$
4.9	$-1.128 \cdot 10^{-3}$	$-7.243 \cdot 10^{-3}$	$-2.139 \cdot 10^{-2}$
5	$-9.821 \cdot 10^{-4}$	$-6.397 \cdot 10^{-3}$	$-1.958 \cdot 10^{-2}$
5.1	$-8.538 \cdot 10^{-4}$	$-5.655 \cdot 10^{-3}$	$-1.794 \cdot 10^{-2}$
5.2	$-7.412 \cdot 10^{-4}$	$-5.003 \cdot 10^{-3}$	$-1.645 \cdot 10^{-2}$
5.3	$-6.428 \cdot 10^{-4}$	$-4.428 \cdot 10^{-3}$	$-1.508 \cdot 10^{-2}$
5.4	$-5.571 \cdot 10^{-4}$	$-3.921 \cdot 10^{-3}$	$-1.383 \cdot 10^{-2}$
5.5	$-4.827 \cdot 10^{-4}$	$-3.473 \cdot 10^{-3}$	$-1.266 \cdot 10^{-2}$
5.6	$-4.182 \cdot 10^{-4}$	$-3.077 \cdot 10^{-3}$	$-1.158 \cdot 10^{-2}$
5.7	$-3.624 \cdot 10^{-4}$	$-2.724 \cdot 10^{-3}$	$-1.058 \cdot 10^{-2}$
5.8	$-3.143 \cdot 10^{-4}$	$-2.411 \cdot 10^{-3}$	$-9.632 \cdot 10^{-3}$
5.9	$-2.727 \cdot 10^{-4}$	$-2.133 \cdot 10^{-3}$	$-8.750 \cdot 10^{-3}$
6	$-2.368 \cdot 10^{-4}$	$-1.884 \cdot 10^{-3}$	$-7.922 \cdot 10^{-3}$

Table S3 Continued.

Distance r (Å)	Dimer Si-He	Si-Ar	Si-Xe
6.5	$-1.193\cdot10^{-4}$	$-9.851\cdot10^{-4}$	$-4.493\cdot10^{-3}$
7	$-6.264\cdot10^{-5}$	$-4.669\cdot10^{-4}$	$-2.056\cdot10^{-3}$
7.5	$-3.449\cdot10^{-5}$	-	-
8	$-1.990\cdot10^{-5}$	-	-
8.5	$-1.201\cdot10^{-5}$	-	-
9	$-7.541\cdot10^{-6}$	-	-
9.5	$-4.909\cdot10^{-6}$	-	-
10	$-3.299\cdot10^{-6}$	-	-

We found that the fitting range for all dimers with exception of the He-He dimer can be extended towards even smaller values of $r_{\mathrm{f,min}}$ by using a larger number of data points at $r \lesssim r_{\mathrm{f,min}}$ with reduced spacing Δr. Moreover, even the current MLR potentials, with exception of the He-He potential, can be used at least as first-order approximations at $r < r_{\mathrm{f,min}}$, as Δ_i remains relatively small at $r \approx r_{\mathrm{f,min}}$. For the He-He dimer, the use of additional data points in the range 0.2 Å $\leq r \leq$ 1 Å results in either a PEC with additional extrema or does not allow to increase the accuracy of the fitting function at $r <$ 0.6 Å, where the MLR potential strongly overestimates the energy. For the current MLR potential of the He-He dimer, $|\Delta_i| < 0.07$ at $r \geq$ 0.53 Å, but it grows fast with decreasing distance at $r <$ 0.53 Å.

To find the parameters of the MLR potential for the Xe-Xe dimer in Table 3, the functional representation of the potential energy $V(r)$ of the Xe-Xe PEC obtained in ref. S4 in the form

$$V(r) = A\exp\left(a_1 r + a_2 r^2 + \frac{a_{-1}}{r} + \frac{a_{-2}}{r^2}\right) - \sum_{n=3}^{8}\left[\frac{C_{2n}}{r^{2n}}\left(1 - \exp(-br)\sum_{k=0}^{2n}\frac{(br)^k}{k!}\right)\right] \qquad \text{(S2)}$$

was used. This functional form is a modification of the potential function developed by Tang & Toennies (2003).[S5] In eqn (S2), C_{2n} are the dispersion coefficients, and A and b are the Born-Mayer parameters. The higher dispersion coefficients, C_{12}, C_{14}, and C_{16} are determined by the recursion equation:

$$C_{2n} = C_{2n-6}\left(\frac{C_{2n-2}}{C_{2n-4}}\right)^3, \quad n = 6,7,8. \qquad \text{(S3)}$$

Table S4 Range of the interatomic distance $r_{\mathrm{f,min}} \le r \le r_{\mathrm{f,max}}$, where the results of the QMC calculations are used to find the best-fit parameters of the MLR potentials in Table 3, value $V_{\mathrm{f,min}} = V(r_{\mathrm{f,min}})$, and relative RMS deviation for the MLR and LJ potentials calculated based on eqn (6) at $r_{\mathrm{f,min}} \le r \le r_{\mathrm{f,max}}$, for all dimers considered in the present work. For the Xe-Xe dimer, the QMC data points were obtained on a mesh with equal spacing from the PEC in the functional form suggested in ref. S4, eqn (S2). Other parameters presented in the table characterize the relevant minimum interatomic distance for calculations of the deflection angles at an equivalent temperature of $T_{**} = 10^5$ K (here, $3k_B T_{**}/2 = m_{12} C_{r*}^2 */2 = V(r_{**}) = 12.93$ eV) or collision velocity C_{r*} (here, $mC_{r*}^2/2 = 3k_B T_*/2 = V(r_*) = V_*$), where m is the reduced mass of the corresponding atom pair.

Dimer	$r_{\mathrm{f,min}}$ (Å)	$r_{\mathrm{f,max}}$ (Å)	$V_{\mathrm{f,min}}$ (eV)	MLR RMS	LJ RMS	$T_{**} = 10^5$ K		$T_* = mC_{r*}^2/(3k_B)$			
						C_{r**} (kms^{-1})	r_{**} (Å)	C_{r*} (kms^{-1})	T_* ($\times 10^3$K)	r_* (Å)	V_* (eV)
He-He	0.6	8.0	18.89	$3.29\cdot10^{-2}$	$1.75\cdot10^{3}$	35.30	0.7177	28	62.90	0.8258	8.131
Ar-Ar	1.1	7.5	66.02	$4.80\cdot10^{-2}$	$7.44\cdot10^{1}$	11.17	1.669	12	115.3	1.623	14.91
Xe-Xe	1.2	9.0	250.5	$4.76\cdot10^{-3}$	$8.15\cdot10^{1}$	6.164	2.109	12	379	1.617	48.99
Cu-Cu	0.6	5	514.5	$4.18\cdot10^{-2}$	$3.69\cdot10^{3}$	8.860	1.383	12	183.4	1.268	23.71
Cu-He	2.0	10	2759	$2.09\cdot10^{-2}$	$8.06\cdot10^{-1}$	25.74	2.838	24	86.95	2.861	11.24
Cu-Ar	1.7	7.0	20.61	$1.27\cdot10^{-2}$	6.65	10.08	1.770	12	141.6	1.721	18.30
Cu-Xe	1.0	7.0	147.1	$4.38\cdot10^{-3}$	$7.31\cdot10^{1}$	7.632	1.601	12	247.2	1.381	31.95
Si-Si	1.0	9	47.18	$9.08\cdot10^{-3}$	$2.10\cdot10^{2}$	13.33	1.323	12	81.07	1.364	10.48
Si-He	1.2	6	1131	$1.84\cdot10^{-2}$	2.41	26.68	1.576	24	80.90	1.589	10.46
Si-Ar	1.1	6	8442	$1.71\cdot10^{-2}$	7.11	12.30	1.765	12	95.21	1.771	12.31
Si-Xe	1.1	7	92.89	$2.87\cdot10^{-2}$	$5.55\cdot10^{1}$	10.38	1.674	12	133.6	1.594	17.27

Table S5 Potential parameters for the Xe-Xe dimer in eqn (S2).[S4]

Potential parameter	Value	Unit
A	57931707.1	K
a_1	-2.08311994	Å^{-1}
a_2	-0.147746919	Å^{-2}
a_{-1}	-2.89687722	Å
a_{-2}	2.58975595	Å^2
b	2.4433788	Å^{-1}
C_6	2002980.34	KÅ^6
C_8	19913048.1	KÅ^8
C_{10}	289841040	KÅ^{10}

The values of the parameters in eqn (S2) are listed in Table S5. These parameters were determined in ref. S4 by fitting the energy values established in the CCSD(T) calculations. The parameters in Table S5 correspond to a potential well depth D_e of 0.02408 eV and equilibrium interatomic distance r_e of 4.378 Å.

Equation (S2) was used to generate an array of energy values with the increment of interatomic distance equal to $\Delta r = 0.01$ Å. The parameters of the MLR potential then were determined based on the array of generated data points by the multifactorial non-linear least-square fitting, which was used to find the MLR potential parameters for other dimers in Table 3. The obtained MLR potential is shown by the solid curve in Fig. S4, where other curves correspond to analytical potentials for the Xe-Xe dimer suggested in ref. S4-S6, and the crosses represent data points found in the CCSD(T) calculations in ref. S4.

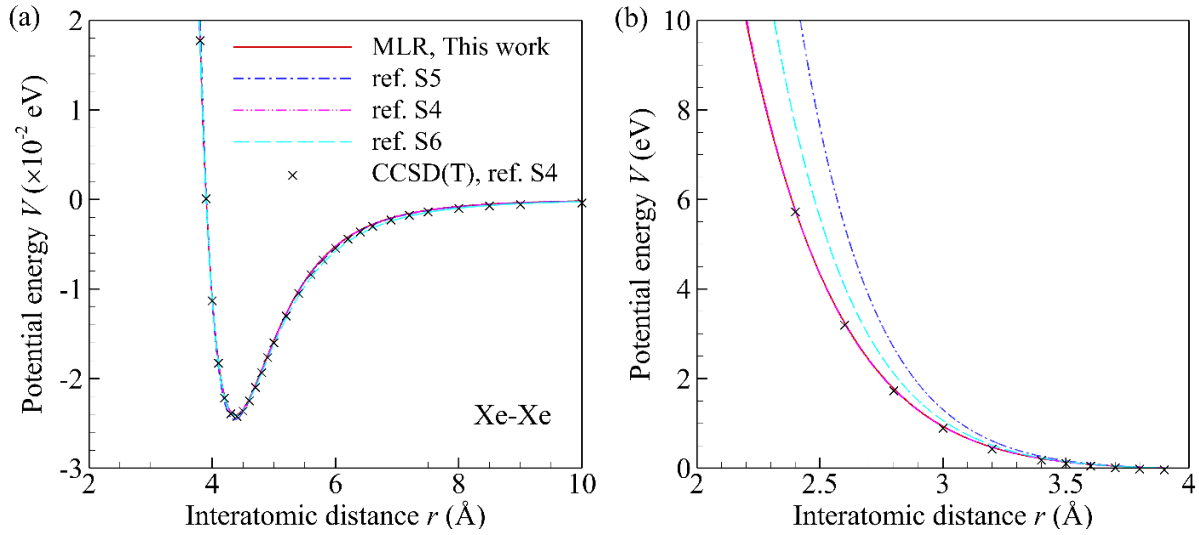

Fig. S4 Potential energy of the Xe-Xe dimer calculated based on the MLR potential developed in the present work (red solid curves) and analytical potential functions suggested in ref. S5 (blue dashed-dotted curve), S4 (magenta dashed-double-dotted curve), and S6 (cyan long-dashed curve). The crosses correspond to the values of energy obtained in the CCSD(T) calculations in ref. S4. Panels (a) and (b) show the same data on different scales along x- and y-axes. The red solid and magental dashed-double-dotted curves visually coincide with each other.

S4. Comparison of calculated PECs for dimers involving copper and silicon atoms with the literature data

The calculated PECs for homo- and heteronuclear dimers containing Cu and Si atoms are compared with the data available from the literature in Fig. S5 and S6. Table 2 also contains the values of the potential well depth D_e and equilibrium distance r_e obtained in the present work and ref. S4-S12 for various dimers.

For the Cu-Cu dimer [Fig. S5(a)], the QMC PEC found in the present work agrees well with the PEC found based on the DFT calculations with van der Waals corrections in ref. S7. Overall, these results are also in close agreement with the results of the CCSD(T) calculations performed in ref. S8 with exception of a vicinity of the equilibrium distance, $r = r_e$. The calculations in ref. S8 predict ~13% smaller D_e as compared to the values found in the present work and in ref. S7.

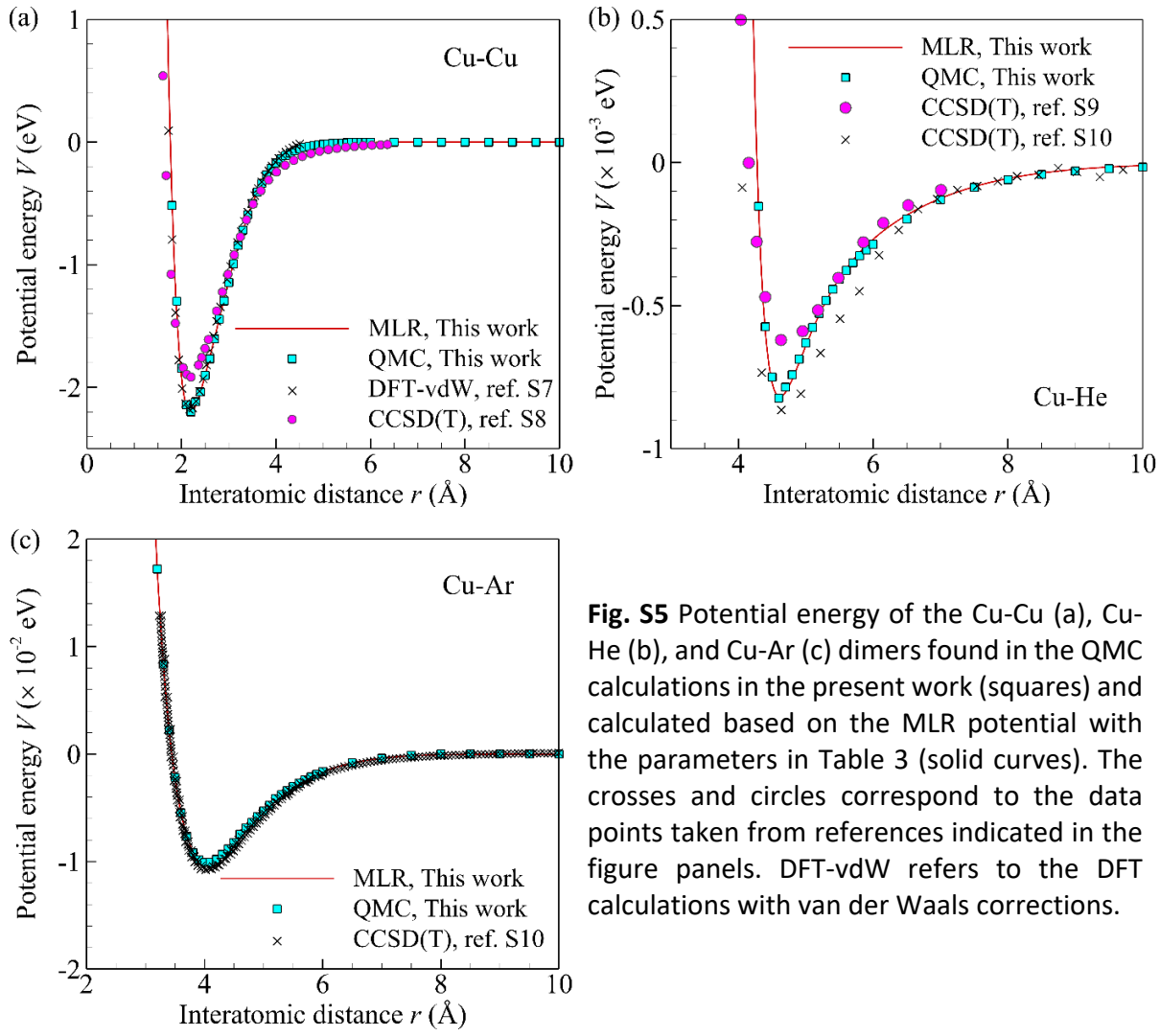

Fig. S5 Potential energy of the Cu-Cu (a), Cu-He (b), and Cu-Ar (c) dimers found in the QMC calculations in the present work (squares) and calculated based on the MLR potential with the parameters in Table 3 (solid curves). The crosses and circles correspond to the data points taken from references indicated in the figure panels. DFT-vdW refers to the DFT calculations with van der Waals corrections.

The PECs for the Cu-He dimer [Fig. S5(b)] known from the literature are currently characterized by the maximum degree of relative uncertainty compared to other dimers considered in Fig. S5 and S6. The PEC found in the QMC calculations in the present work is in between the PECs found in the CCSD(T) calculations in ref. S9 and S10. All three sets predict nearly the same value of r_e. The value of D_e obtained in the present work agrees well with the value found in ref. S10, while the value obtained in ref. S9 is ~24% smaller. At the same time, the calculations performed in ref. S10 predict less stiff PEC at both attraction and repulsion branches compared to the PEC obtained in the present work. It is worth noting, however, that the data points from ref. S10 shown by crosses in Fig. S5(b) are obtained by digitizing a curve provided in the original paper. Due to the small scale of the original picture, the obtained energy values presumably

include additional errors compared to the values used for the preparation of the corresponding picture in ref. S10.

For the Cu-Ar dimer [Fig. S5c)], the energy values calculated in the present work are in close agreement with the energies obtained in ref. S10 in the whole range of interatomic distances under consideration. For the Si-Si [Fig. S6(a)] and Si-Ar [Fig. S6(b)] dimers, the energy values agree well with the results of calculations in ref. S11 and S12, respectively.

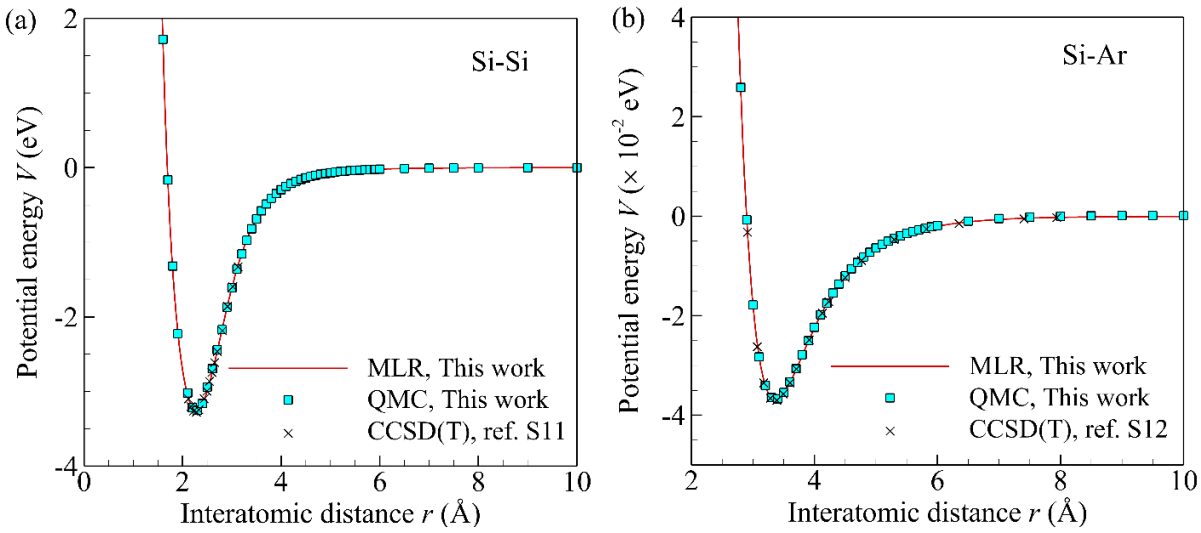

Fig. S6 Potential energy of the Si-Si (a) and Si-Ar (c) dimers found in the QMC calculations in the present work (squares) and calculated based on the MLR potential with the parameters in Table 3 (solid curves). The crosses correspond to the data points taken from the references indicated in the figure panels.

It is clear from the results shown in Fig. S5 and S6 that the PECs available from the literature often lack data points at relatively small and relatively large interatomic distances. To predict the transport coefficients of gaseous mixtures in a broad range of temperature, accurate information about the PEC in a broad range of r is vital. The QMC calculations performed in the present work are targeted at filling this gap and opening the way for high-fidelity calculations of the transport coefficients and parameters of molecular models such as variable hard sphere (VHS)[S13] and variable soft sphere (VSS)[S14] models for the gaseous mixtures under consideration.

It is apparent from the comparison of the PECs shown in Fig. 1 and S4 and comparison of D_e and r_e in Table 2 for the homonuclear He-He, Ar-Ar, and Xe-Xe dimers that the PECs for these dimers obtained in the various works, including the present paper, are consistent with each other

in the range of large and moderate distances. At small distances, however, the data points are lacking, and, therefore, the PECs in various functional forms suggested in the literature can deviate from each other.

S5. Effect of the PEC shape on scattering of atoms in binary collisions

Figures S7-S17 shows characteristic distributions of the quantity $\vartheta = 1 - \cos\chi$ *versus* b^2 for all atom pairs considered in the present paper, calculated based on the MLR (red solid curves) and Lennard-Jones (LJ) (green dashed curve) potentials. In addition, for the He-He (Fig. S7), Ar-Ar (Fig. S8), and Xe-Xe (Fig. S9) atom pairs, the values of ϑ calculated based on the potential functions developed in ref. S4-S6 and S15 are shown. For the convenience of comparison, Fig. S8, S10, and S12 reproduce the same data as Fig. 4-6.

The relationships between distributions of ϑ obtained based on the MLR and LJ potentials are consistent over all atom pairs. There is a notable qualitative agreement between distributions of ϑ obtained based on the LJ and MLR potentials at each relative speed C_r considered. Quantitatively, the values ϑ calculated based on the LJ potential demonstrate the strongest deviation from ϑ calculated based on MLR potential at the smallest [20 ms^{-1}, panels (a)] and largest [10^4 ms^{-1}, panels (d)] C_r, while at the intermediate C_r [10^3 ms^{-1}, panels (c)], the dependence of ϑ on b^2 is practically independent of the shape of the potential function. The range of b^2 corresponding to quasi-orbiting collisions predicted by the LJ potential is shifted towards larger values of b^2 compared to predictions based on the MLR potential.

For all atom pairs with exception of the Cu-He pair, the LJ potential overestimates the energy compared to the MLR potential at both attraction and repulsion and, correspondingly, the values of ϑ calculated based on LJ potential for nearly head-on collisions are greater than the values predicted based on the MLR potential for the corresponding atom pairs considered at small and large C_r. For the Cu-He atom pair, the LJ potential underestimates the energy at repulsion [Fig. 2(b)] and, correspondingly, underestimates ϑ at large C_r [Fig. S12(c) and (d)].

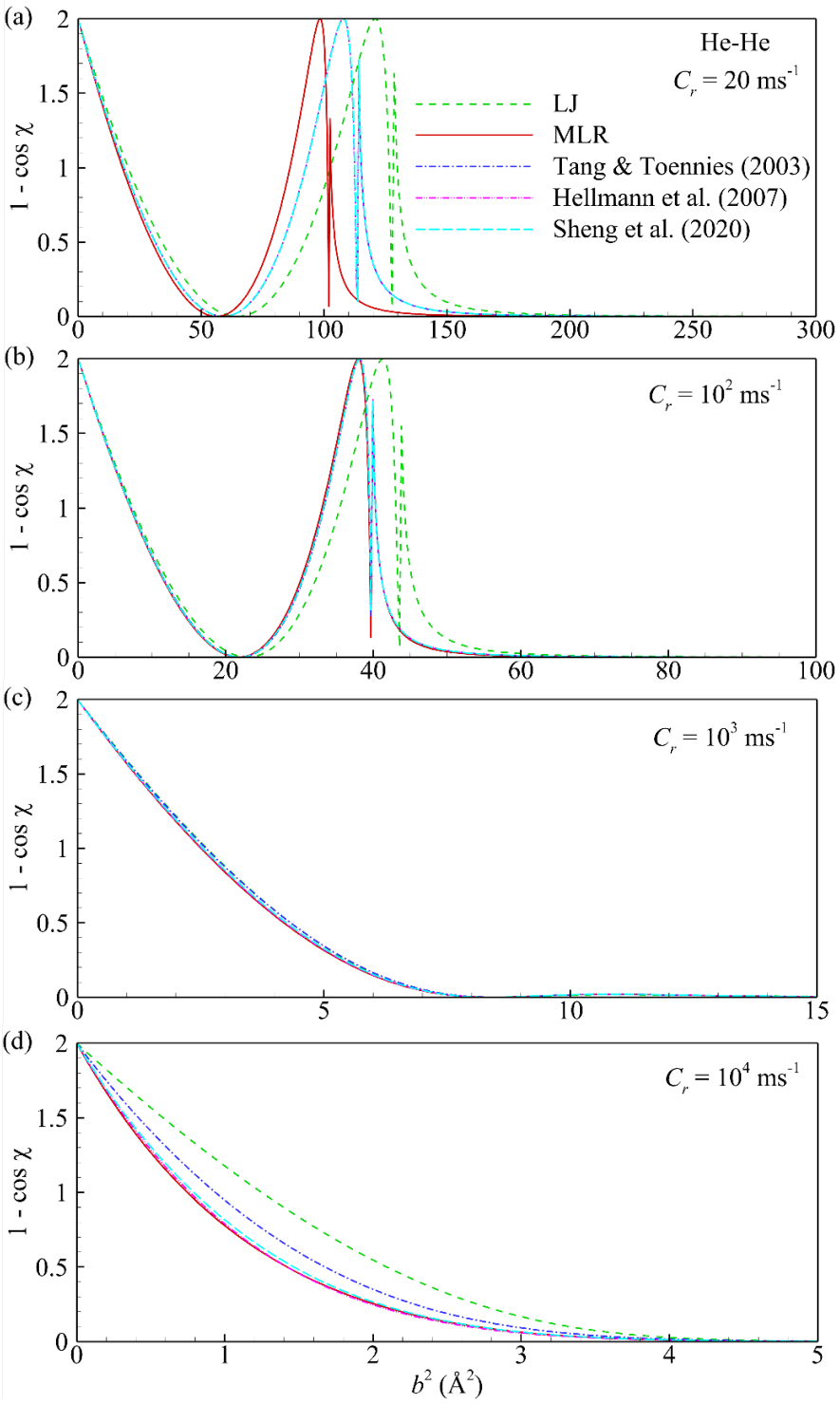

Fig. S7 Quantity $1 - \cos\chi$, where χ is the deflection angle defined by eqn (8), *versus* b^2 for two He atoms at a relative speed C_r of 20 ms^{-1} (a), 10^2 ms^{-1} (b), 10^3 ms^{-1} (c), and 10^4 ms^{-1} (d) calculated based on the MLR (solid curves) and LJ (dashed curves) potentials. Other curves are obtained based on the potential functions suggested in the literature as indicated in panel (a).

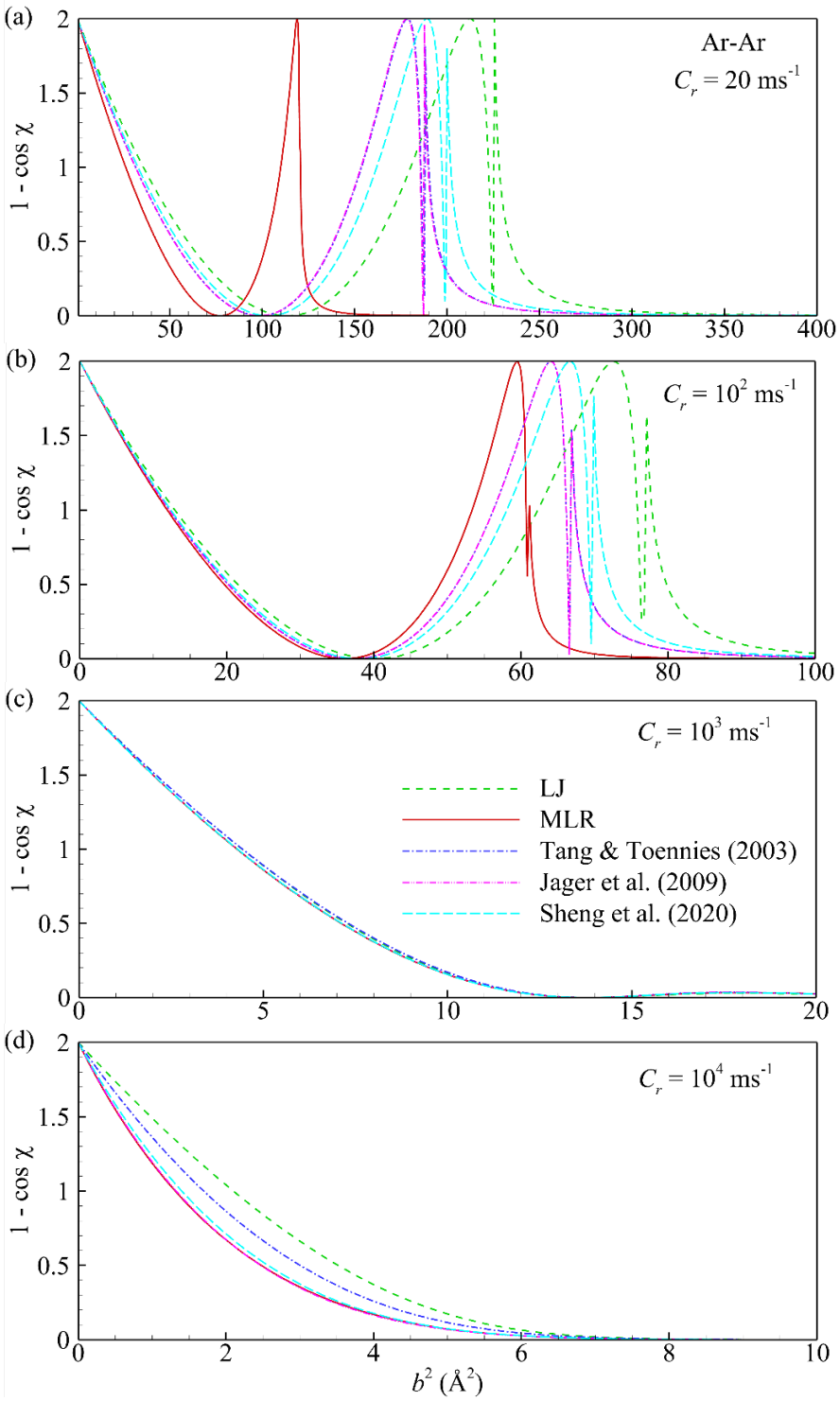

Fig. S8 Quantity $1 - \cos\chi$, where χ is the deflection angle defined by eqn (8), *versus* b^2 for two Ar atoms at a relative speed C_r of 20 ms^{-1} (a), 10^2 ms^{-1} (b), 10^3 ms^{-1} (c), and 10^4 ms^{-1} (d) calculated based on the MLR (solid curves) and LJ (dashed curves) potentials. Other curves are obtained based on the potential functions suggested in the literature as indicated in panel (c).

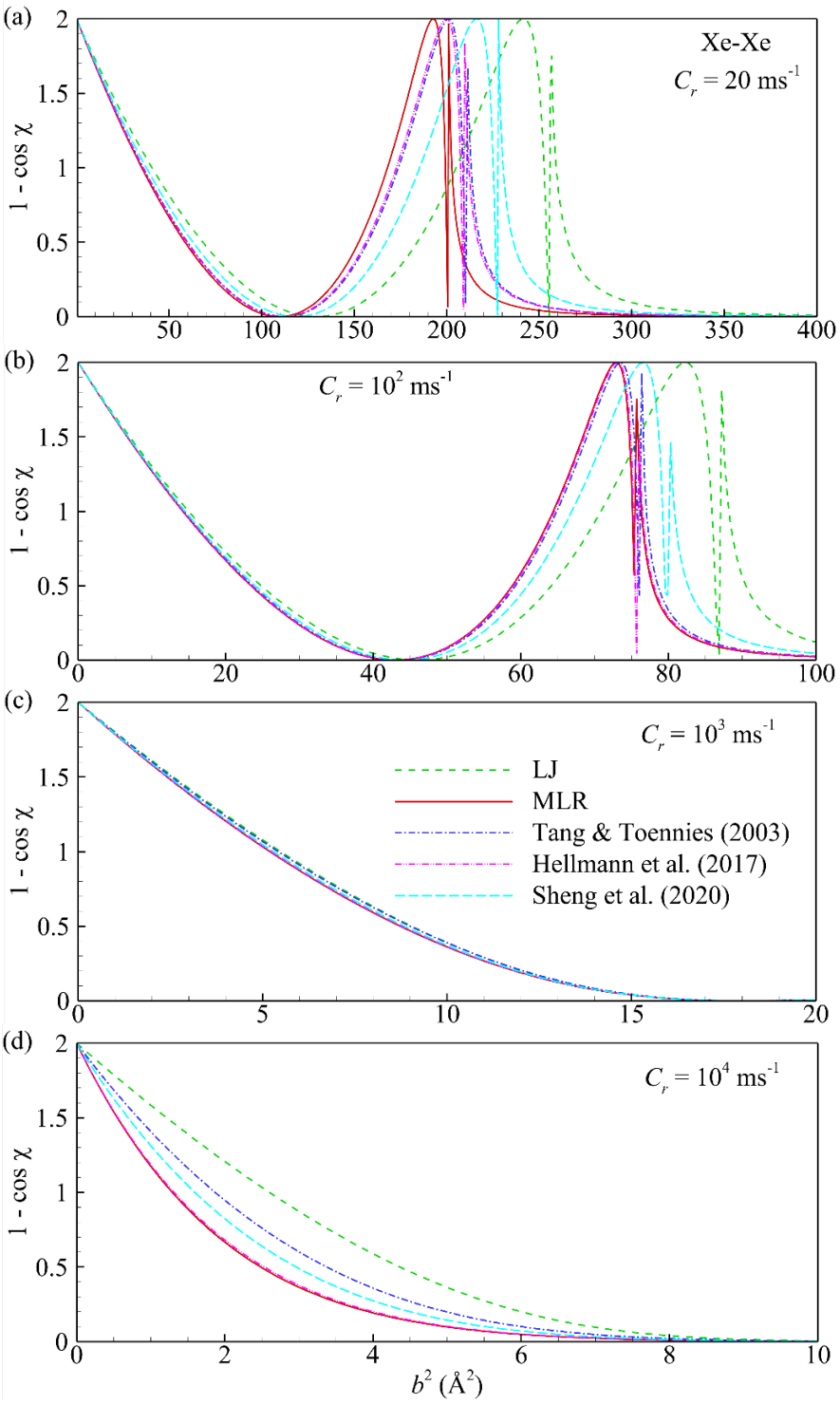

Fig. S9 Quantity $1 - \cos\chi$, where χ is the deflection angle defined by eqn (8), *versus* b^2 for two Xe atoms at a relative speed C_r of 20 ms^{-1} (a), 10^2 ms^{-1} (b), 10^3 ms^{-1} (c), and 10^4 ms^{-1} (d) calculated based on the MLR (solid curves) and LJ (dashed curves) potentials. Other curves are obtained based on the potential functions suggested in the literature as indicated in panel (c).

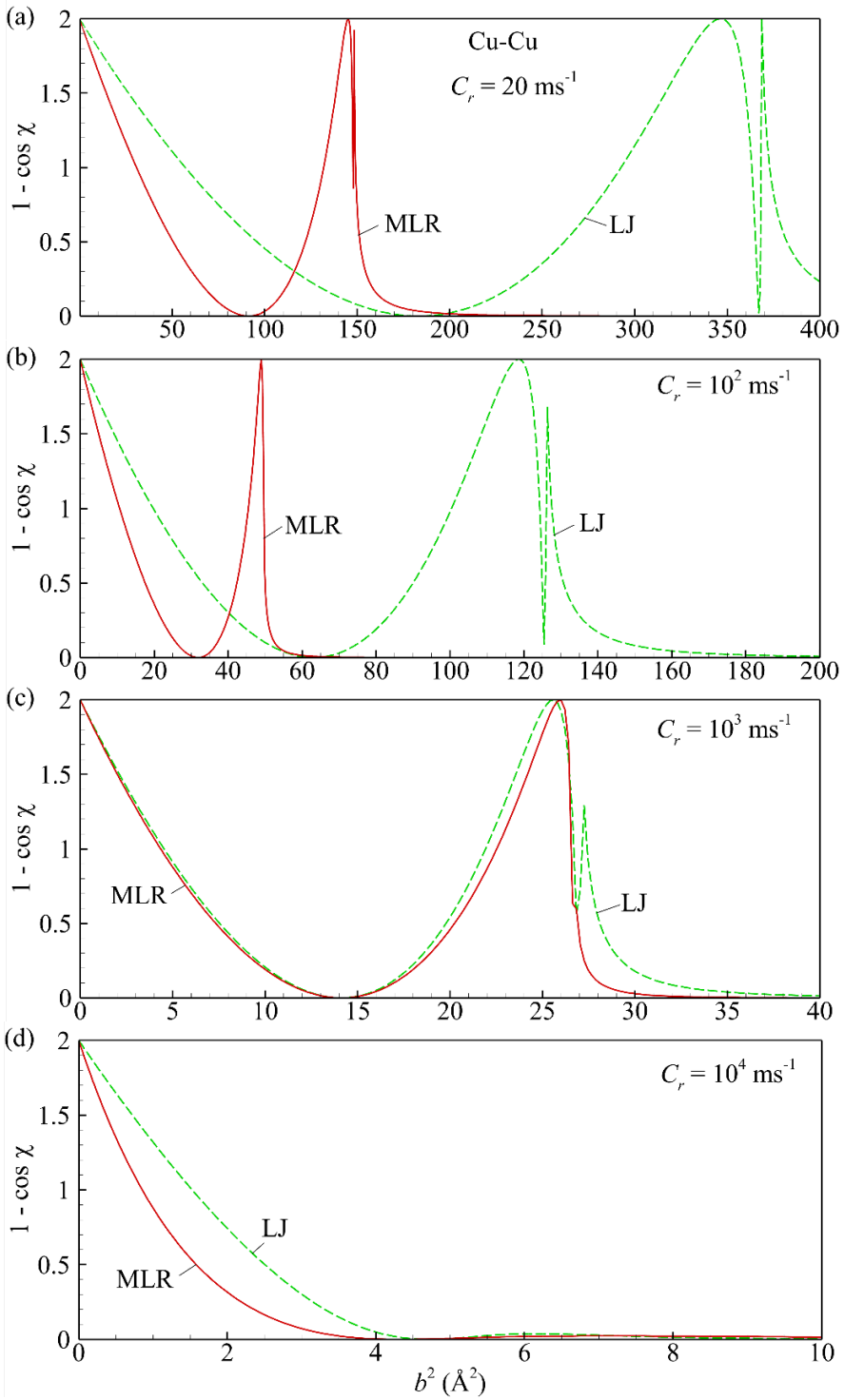

Fig. S10 Quantity $1 - \cos\chi$, where χ is the deflection angle defined by eqn (8), *versus* b^2 for two Cu atoms at a relative speed C_r of 20 ms^{-1} (a), 10^2 ms^{-1} (b), 10^3 ms^{-1} (c), and 10^4 ms^{-1} (d) calculated based on the MLR (solid curves) and LJ (dashed curves) potentials.

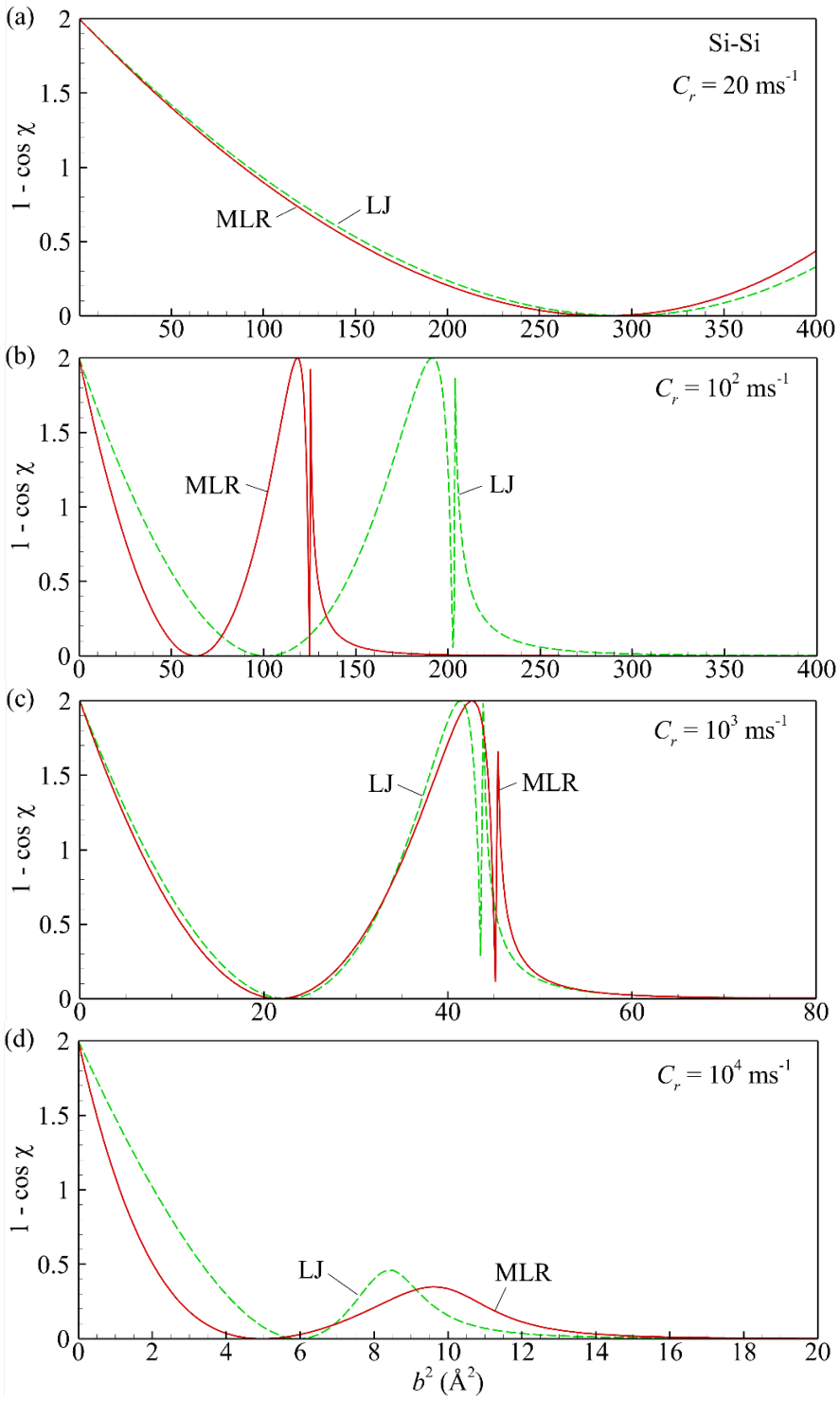

Fig. S11 Quantity $1 - \cos\chi$, where χ is the deflection angle defined by eqn (8), *versus* b^2 for two Si atoms at a relative speed C_r of 20 ms^{-1} (a), 10^2 ms^{-1} (b), 10^3 ms^{-1} (c), and 10^4 ms^{-1} (d) calculated based on the MLR (solid curves) and LJ (dashed curves) potentials.

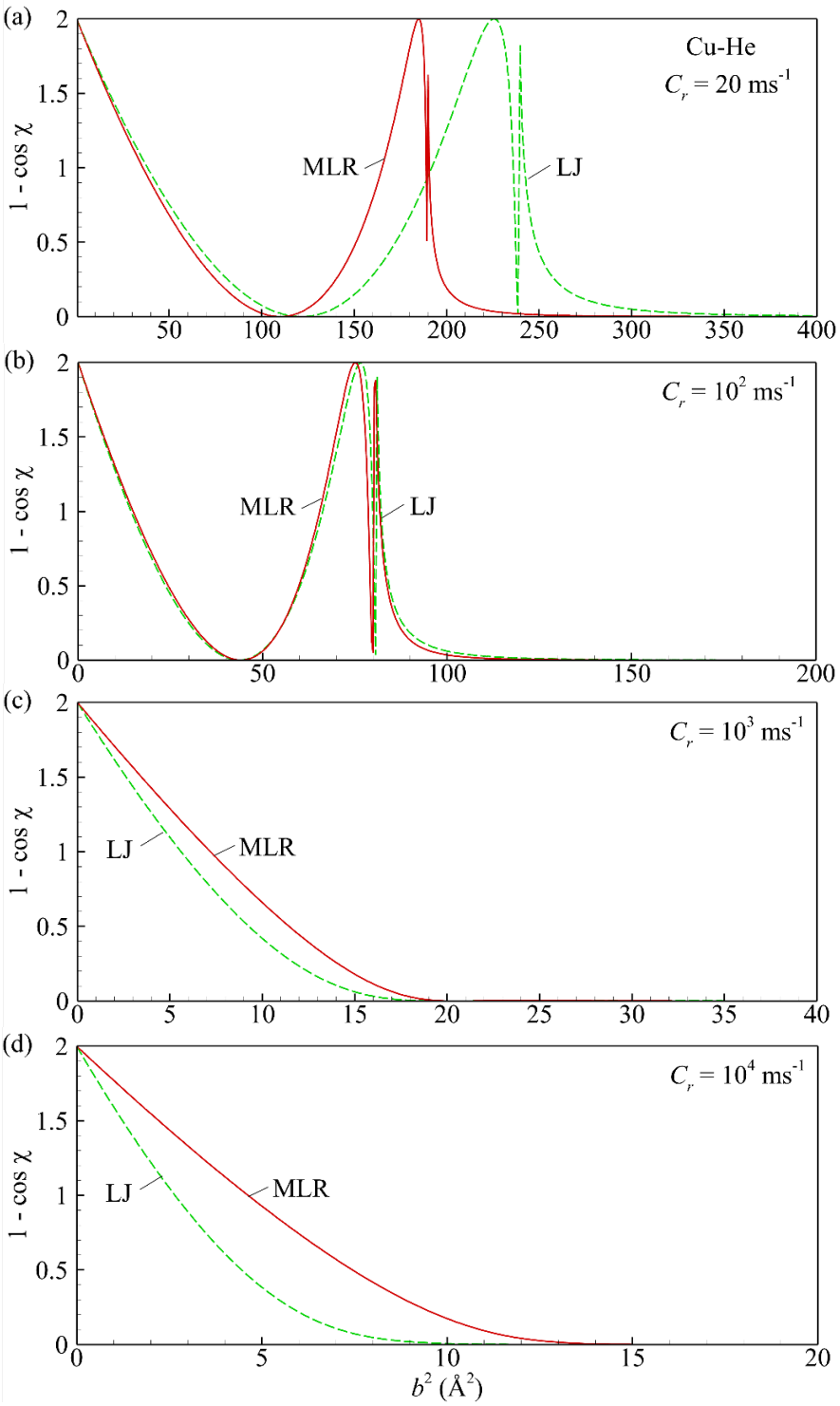

Fig. S12 Quantity $1 - \cos\chi$, where χ is the deflection angle defined by eqn (8), *versus* b^2 for a pair of Cu and He atoms at a relative speed C_r of 20 ms^{-1} (a), 10^2 ms^{-1} (b), 10^3 ms^{-1} (c), and 10^4 ms^{-1} (d) calculated based on the MLR (solid curves) and LJ (dashed curves) potentials.

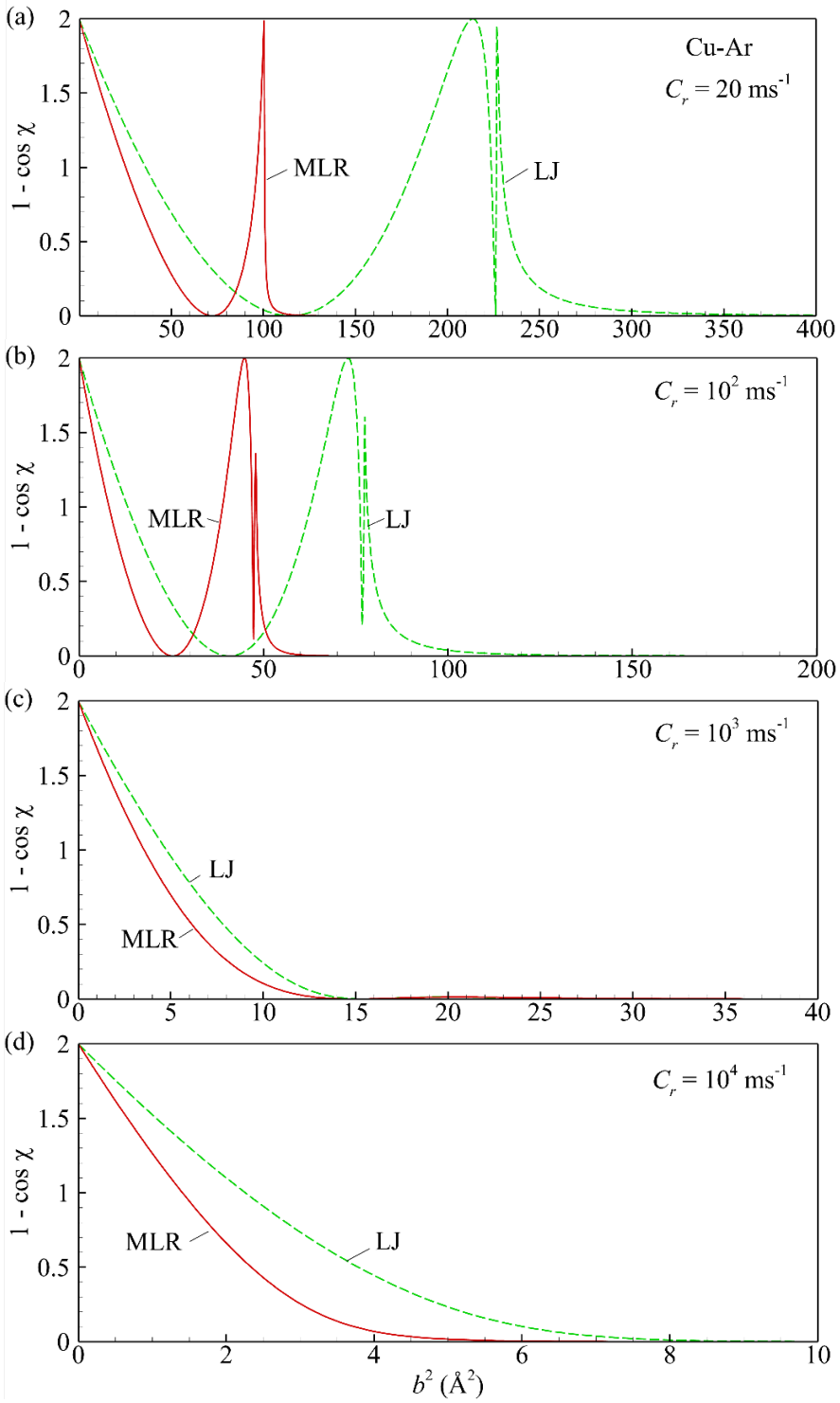

Fig. S13 Quantity $1 - \cos\chi$, where χ is the deflection angle defined by eqn (8), *versus* b^2 for a pair of Cu and Ar atoms at a relative speed C_r of 20 ms^{-1} (a), 10^2 ms^{-1} (b), 10^3 ms^{-1} (c), and 10^4 ms^{-1} (d) calculated based on the MLR (solid curves) and LJ (dashed curves) potentials.

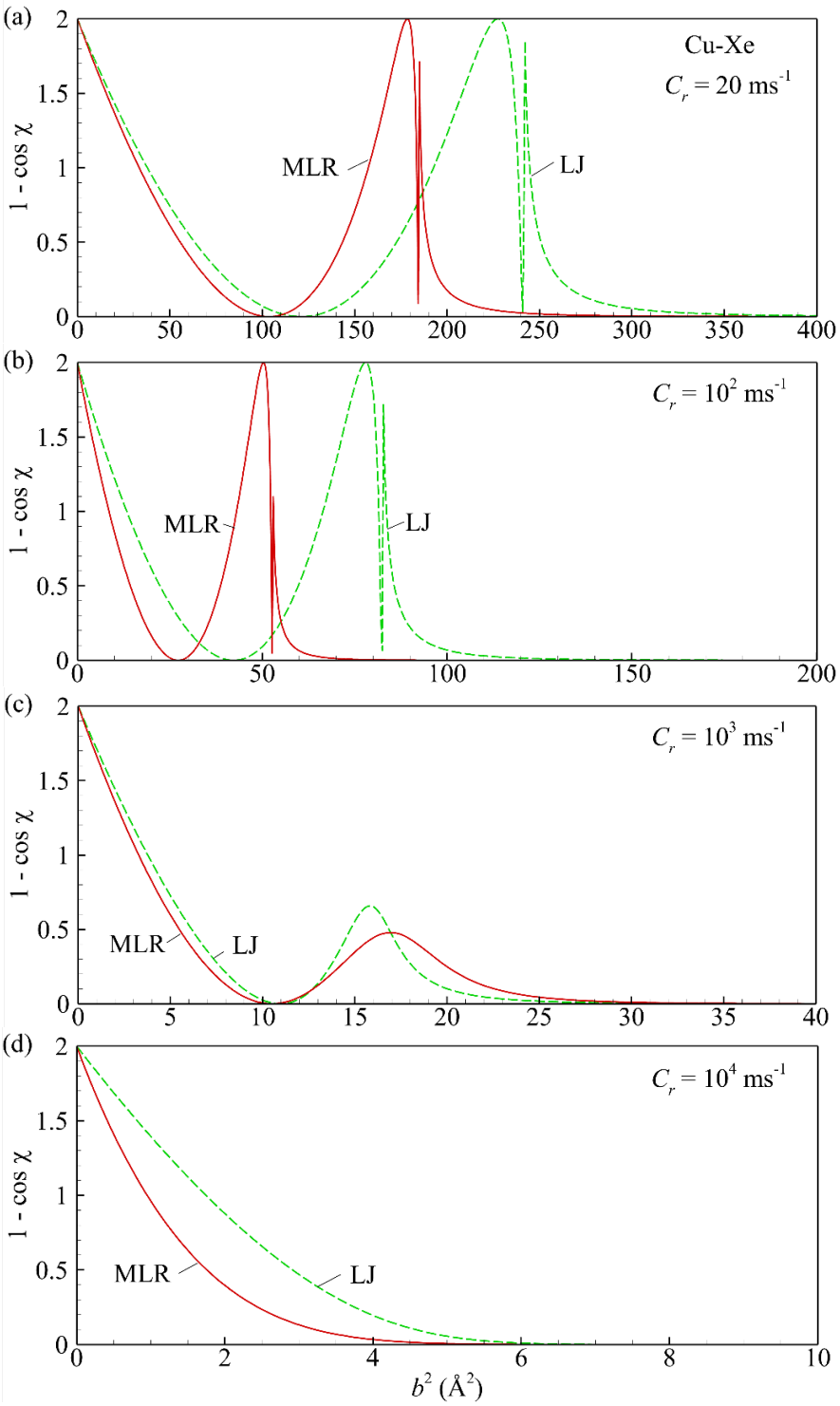

Fig. S14 Quantity $1 - \cos\chi$, where χ is the deflection angle defined by eqn (8), *versus* b^2 for a pair of Cu and Xe atoms at a relative speed C_r of 20 ms^{-1} (a), 10^2 ms^{-1} (b), 10^3 ms^{-1} (c), and 10^4 ms^{-1} (d) calculated based on the MLR (solid curves) and LJ (dashed curves) potentials.

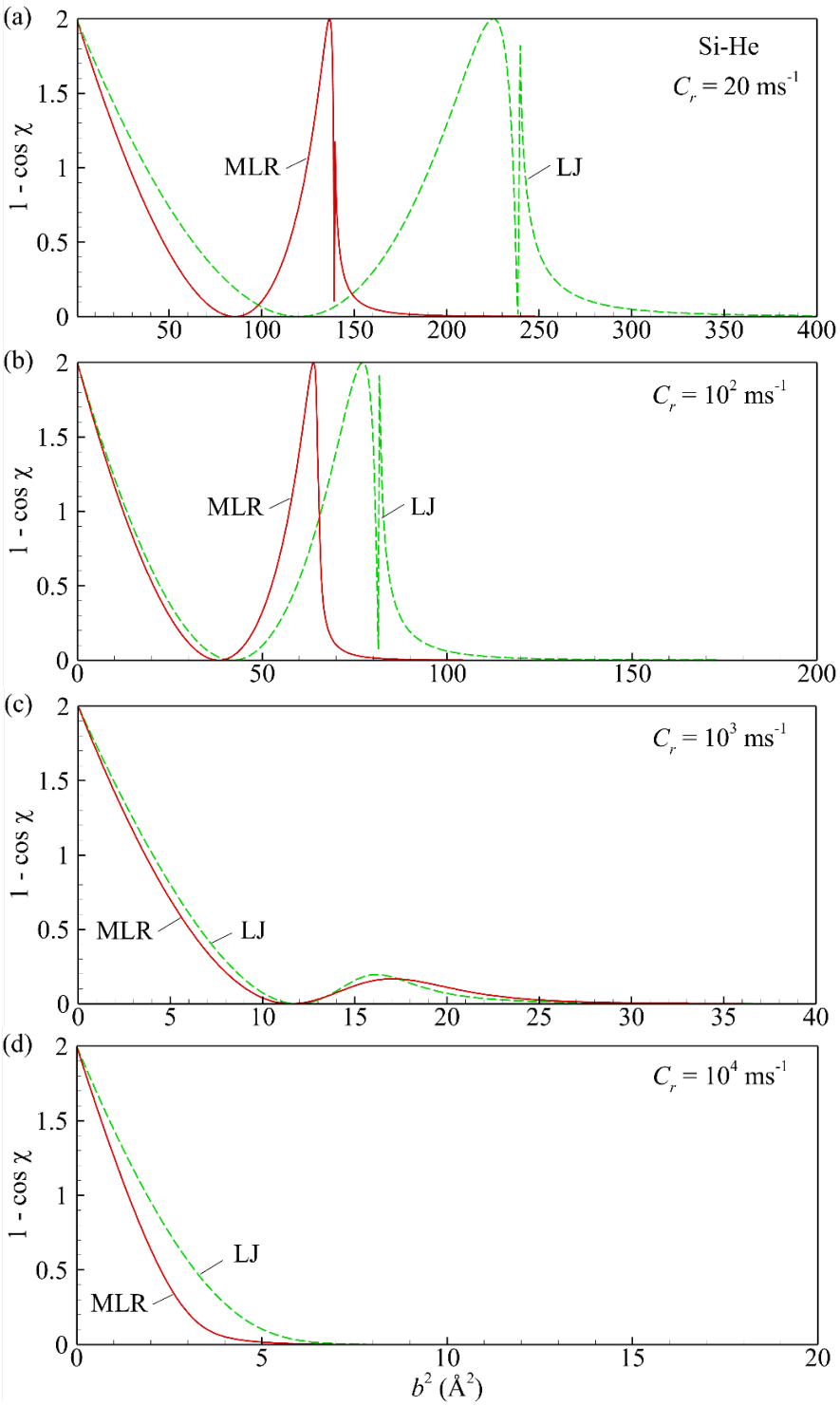

Fig. S15 Quantity $1 - \cos\chi$, where χ is the deflection angle defined by eqn (8), *versus* b^2 for a pair of Si and He atoms at a relative speed C_r of 20 ms^{-1} (a), 10^2 ms^{-1} (b), 10^3 ms^{-1} (c), and 10^4 ms^{-1} (d) calculated based on the MLR (solid curves) and LJ (dashed curves) potentials.

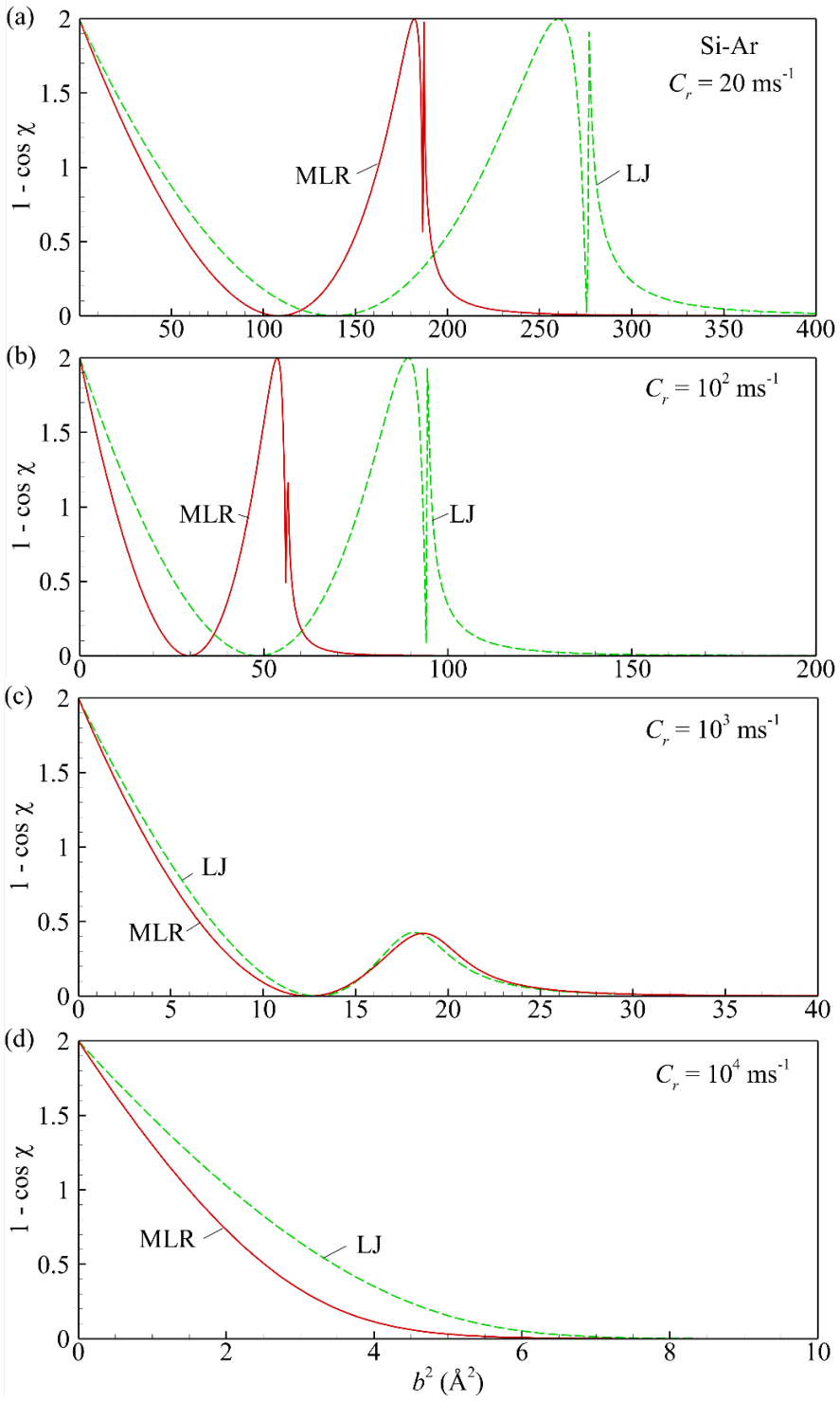

Fig. S16 Quantity $1 - \cos\chi$, where χ is the deflection angle defined by eqn (8), *versus* b^2 for a pair of Si and Ar atoms at a relative speed C_r of 20 ms^{-1} (a), 10^2 ms^{-1} (b), 10^3 ms^{-1} (c), and 10^4 ms^{-1} (d) calculated based on the MLR (solid curves) and LJ (dashed curves) potentials.

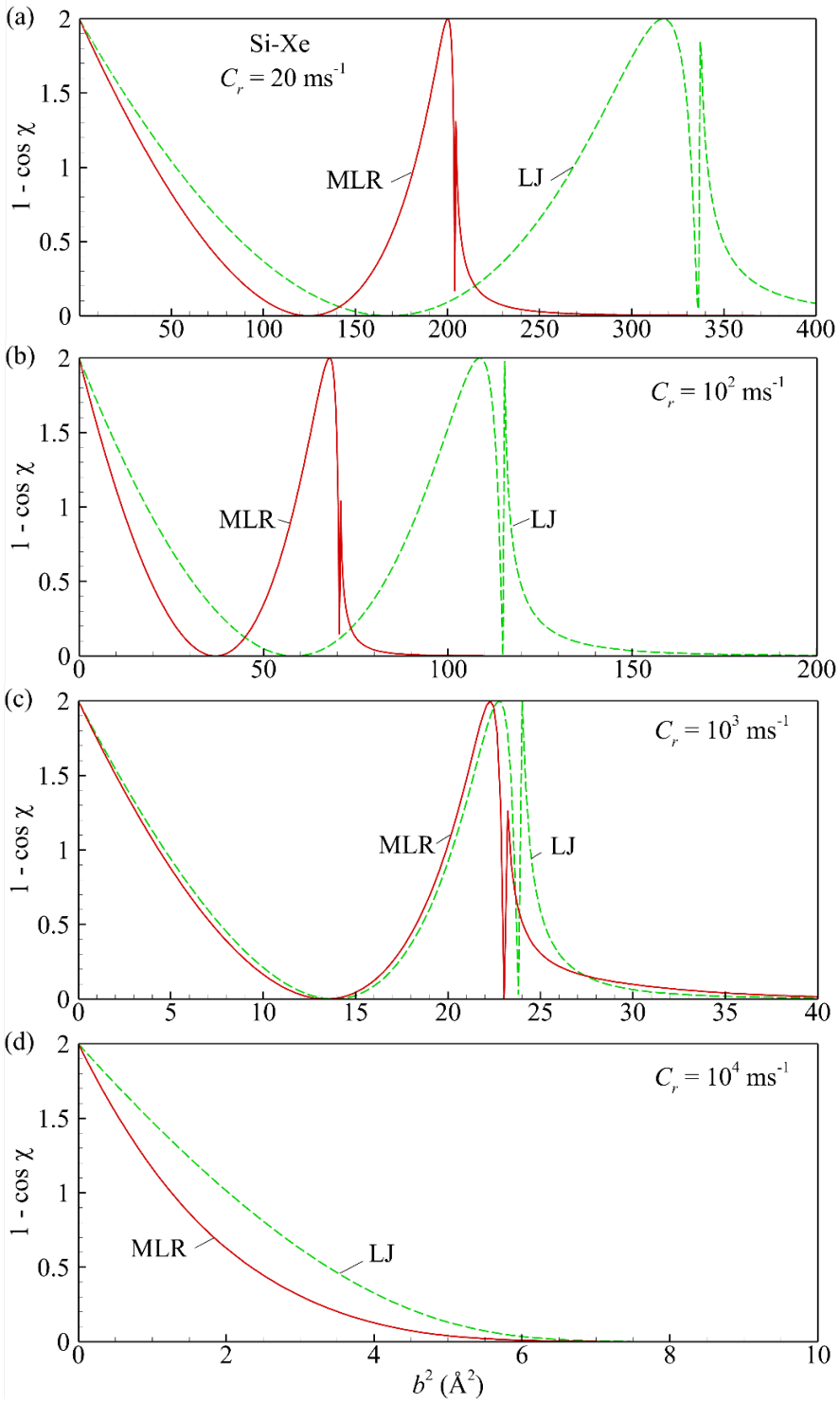

Fig. S17 Quantity $1 - \cos \chi$, where χ is the deflection angle defined by eqn (8), *versus* b^2 for a pair of Si and Xe atoms at a relative speed C_r of 20 ms^{-1} (a), 10^2 ms^{-1} (b), 10^3 ms^{-1} (c), and 10^4 ms^{-1} (d) calculated based on the MLR (solid curves) and LJ (dashed curves) potentials.

S6. Convergence study of numerical calculation of the transport collision integrals and transport coefficients

The numerically calculated values of the transport coefficients primarily depend on the integration step sizes Δb and ΔC_r used for numerical quadrature of the transport collision Ω-integrals in eqn (14)-(15) as well as on the cutoff values of the impact parameter b_* and relative speed C_{r*} that replace the top limits in improper integrals of eqn (14)-(15). The accuracy of the numerical values of the transport coefficients also implicitly depends on the accuracy of the numerical calculation of the deflection angles according to eqn (8).

In the present work, two independently developed codes for calculations of the deflection angle and Ω-integrals were used. The codes use different approaches for numerical quadrature of eqn (8), but it was found the maximum relative difference between $\vartheta = 1 - \cos\chi$ predicted by both codes does not exceed 10^{-6} with exception of sliding collisions at large b, which do not contribute to the Ω-integrals. The first code is based on the numerical quadrature of eqn (14)-(15) on meshes with equal spacings Δb and ΔC_r. The second code utilizes non-homogeneous meshes for both b and C_r.

The results of the convergence study obtained with the code based on the integration with equal spacing Δb and ΔC_r are briefly considered below. To characterize the convergence with respect to some numerical parameter P, the differences between the values of the Ω-integrals calculated at two values P_1 and P_2 of P and the same temperature and other numerical parameters

$$\Delta\left[\Omega^{(l.s)}\right] = \left|\frac{\Omega^{(l.s)}(P_1) - \Omega^{(l.s)}(P_2)}{\Omega^{(l.s)}(P_2)}\right|, \tag{S4}$$

were determined for $l = s = 1$, 2, and 4 at $P_1/P_2 \sim 2$.

The minimum required cutoff value of relative speed C_{r*} strongly depends on the atom pair under consideration. The convergence of the $\Omega^{(2.2)}$ integrals for the He-He and Cu-Cu atom pairs as well as viscosities of He gas and Cu vapor with increasing C_{r*} is illustrated in Fig. S18. Similar convergence studies, which were performed for all other atom pairs, showed that the appropriate C_{r*} must roughly correspond to the equation $mC_{r*}^2/2 = (10 - 20) \times (3k_B T_{\max}/2)$, where m is the reduced mass of the atom pair, $T_{\max} = 10^4$ K is the maximum temperature in the calculations

of the Ω-integrals and transport coefficients, and k_B is the Boltzmann constant. Based on these results, the values of C_{r*} shown in Table S4 were used for numerical integration in eqn (14).

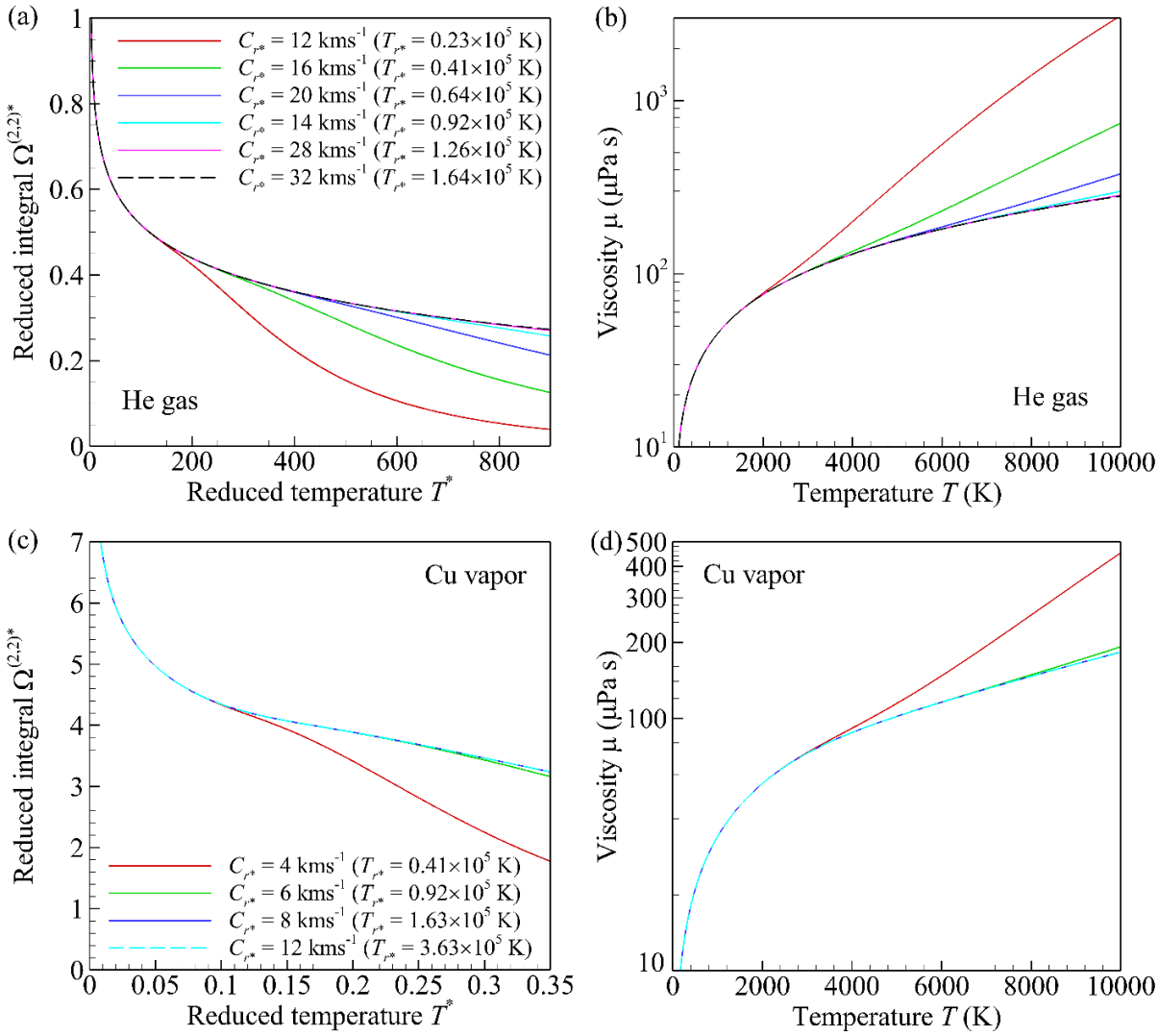

Fig. S18 Reduced integrals $\Omega^{*(2,2)}$ calculated based on the scale $\sigma = r_e/\sqrt[6]{2}$ *versus* reduced temperature $T^* = k_B T/D_e$ (a,c) and viscosity μ *versus* temperature T (b,d) for He gas (a,b) and Cu vapor (c,d) calculated at various values of the cutoff speed C_{r*} that replaces the top limit in the improper integral in eqn (14). The values of C_{r*} are indicated in the figure panels. T_{r*} is the characteristic temperature calculated from the equation $mC_{r*}^2/2 = 3k_B T_*/2$.

The values of $\Delta[\Omega^{(l,s)}]$ at $C_{r*(1)} = 20$ km s^{-1} and $C_{r*(2)} = 12$ km s^{-1} for the Cu-Cu atom pair are shown in Fig. S19(a). These results confirm that $C_{r*} = 12$ km s^{-1} provides the errors in the calculation of the Ω-integrals of the considered orders that are less than 10^{-6}. The same level

of the maximum numerical errors is provided for all atom pairs considered at the values of C_{r*} presented in Table S4.

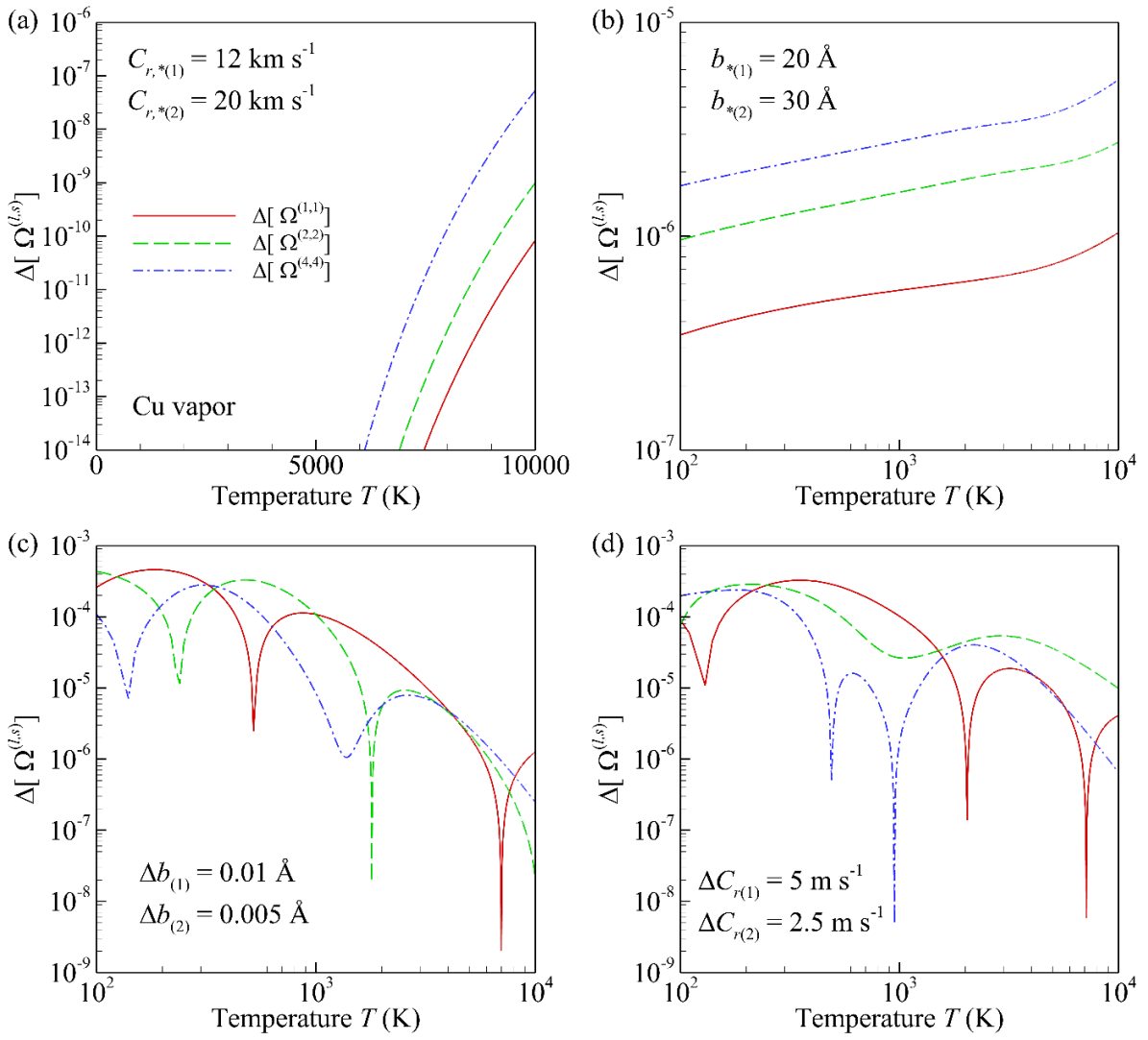

Fig. S19 Values of relative differences $\Delta[\Omega^{(l,s)}]$, eqn (S4), for $l = s = 1$ (red solid curves), $l = s = 2$ (green dashed curves), and $l = s = 4$ (blue dashed-dotted curves) *versus* temperature T for the Cu-Cu atom pair calculated for $P = C_{r*}$ at $C_{r*(1)} = 20$ km s^{-1} and $C_{r*(1)} = 12$ km s^{-1} (a), $P = b_*$ at $b_{*(2)} = 20$ Å and $b_{*(2)} = 30$ Å (b), $P = \Delta b$ at $\Delta b_{(1)} = 0.01$ Å and $\Delta b_{(2)} = 0.005$ Å (c), and $P = \Delta C_r$ at $\Delta C_{r*(1)} = 5$ m s^{-1} and $\Delta C_{r(2)} = 2.5$ m s^{-1} (d).

The effect of b_*, Δb, and ΔC_r on the values of the Ω-integrals is illustrated in Fig. S19(b) and (d) for the Cu-Cu atom pair. These results show that the maximum value of $\Delta[\Omega^{(l,s)}]$ for l and s considered does not exceed $3 \cdot 10^{-6}$ for $P = b_*$ at $b_{*(1)} = 20$ Å and $b_{*(2)} = 30$ Å, $5 \cdot 10^{-4}$

for $P = \Delta b$ at $\Delta b_{(1)} = 0.01$ Å and $\Delta b_{(2)} = 0.005$ Å, as well as $3 \cdot 10^{-4}$ for $P = \Delta C_r$ at $\Delta C_{r(1)} =$ 5 m s^{-1} and $\Delta C_{r(2)} = 2.5$ m s^{-1}. These results are characteristic of all other atom pairs, so that the values of $b_* = 20$ Å, $\Delta b = 0.005$ Å, and $\Delta C_r = 2.5$ ms^{-1} can be chosen for numerical integration in eqn (14)-(15). In this case, the direct calculations showed that the estimated error in the values of all transport coefficients for pure substances does not exceed 0.04% at $T \leq 10^3$ K and 0.01% at $T \geq 10^3$ K.

The results shown in Fig. S19 indicate that the integration step sizes Δb and ΔC_r are the most important factors that limit the numerical accuracy of the transport coefficients if the numerical quadrature is performed on meshes with equal spacing. To solve this issue, the second computational code used in the present work utilizes numerical integration over b and C_r in eqn (14)-(15) at non-uniform meshes. The approach for choosing the numerical parameters for this method is described in ref. S16. For the second code, the estimated relative error of the transport coefficients does not exceed 0.01%.

S7. Transport collision integrals $\Omega^{(1,1)}$ and $\Omega^{(2.2)}$ for various atom pairs and viscosity of noble gases

The values of the reduced transport collision integrals $\Omega^{(1,1)*}$ and $\Omega^{(2.2)*}$ [eqn. (28)] are plotted as functions of the reduced temperature $T^* = k_B T/D_e$ for all atom pairs considered in Fig. S20-S22. The range of the reduced temperature in each plot corresponds to the temperature range from 10 K to 10^4 K. For each pair of colliding atoms, the calculations are performed based on the MLR and LJ potentials. Fig. S21, which shows the values of integrals for atom pairs containing at least one Cu atom, is a copy of Fig. 7 and reproduced here only for the purpose of comparison with the Ω-integrals for other atom pairs.

Overall, the LJ potential provides a poor approximation of the Ω-integrals over a broad temperature range. The agreement between the values of $\Omega^{*(1,1)}$ and $\Omega^{*(2.2)}$ calculated based on the MLR and LJ potentials is usually the best in the intermediate range of the reduced temperature, $\sim 0.1 < T^* < \sim 1$. For atom pairs involving at least one noble gas atom, the agreement also improves with an increasing molecular mass of the participating noble gas atom. The largest disagreement is observed for the He-He [Fig. S20(a)], Cu-He [Fig. S21(b)], and Si-He [Fig. S22(b)] pairs. For the Xe-Xe [Fig. S20(c)], Cu-Xe [Fig. S21(d)], and Si-Xe [Fig. S22(d)] pairs,

the agreement between the results obtained based on the MLR and LJ potentials is the best among all atom pairs considered.

Interestingly, the calculations predict a very large, ~100%, difference between the Ω-integrals calculated based on the MLR and LJ potentials for the Cu-Cu pair at small T^* [Fig. S20(a)]. At the same time, the difference between the Ω-integrals calculated based on the MLR and LJ potentials for the Si-Si atom pair is much smaller [Fig. S21(a)].

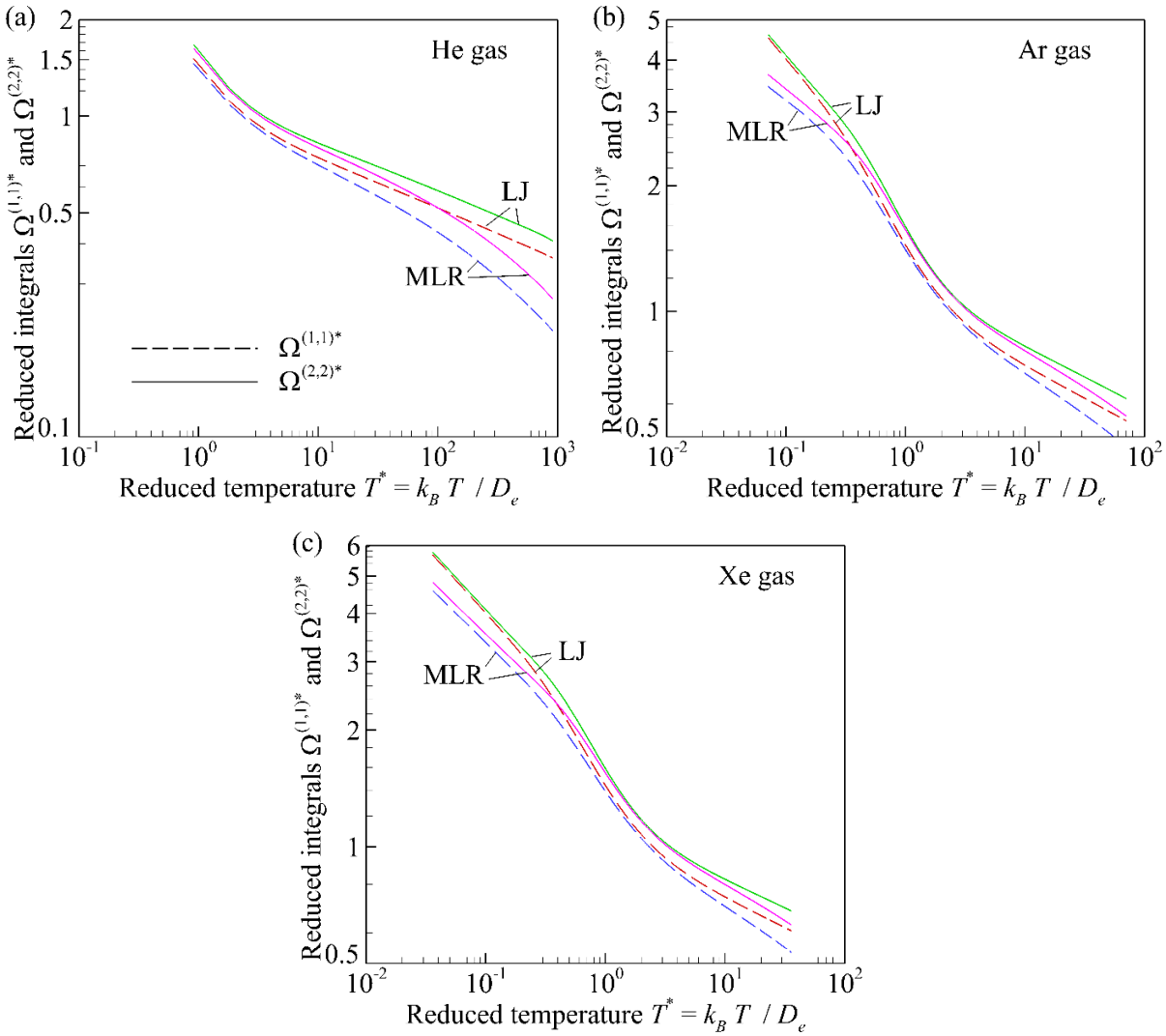

Fig. S20 Reduced integrals $\Omega^{(1.1)*}$ (dashed curves) and $\Omega^{(2.2)*}$ (solid curves) for the He-He (a), Ar-Ar (b), and Xe-Xe (c) atom pairs *versus* reduced temperature $T^* = k_B T/D_e$ calculated based on the LJ (red and green curves) and MLR (blue and magenta curves) potentials. The scale $\sigma = r_e/\sqrt[6]{2}$ is used in eqn (29).

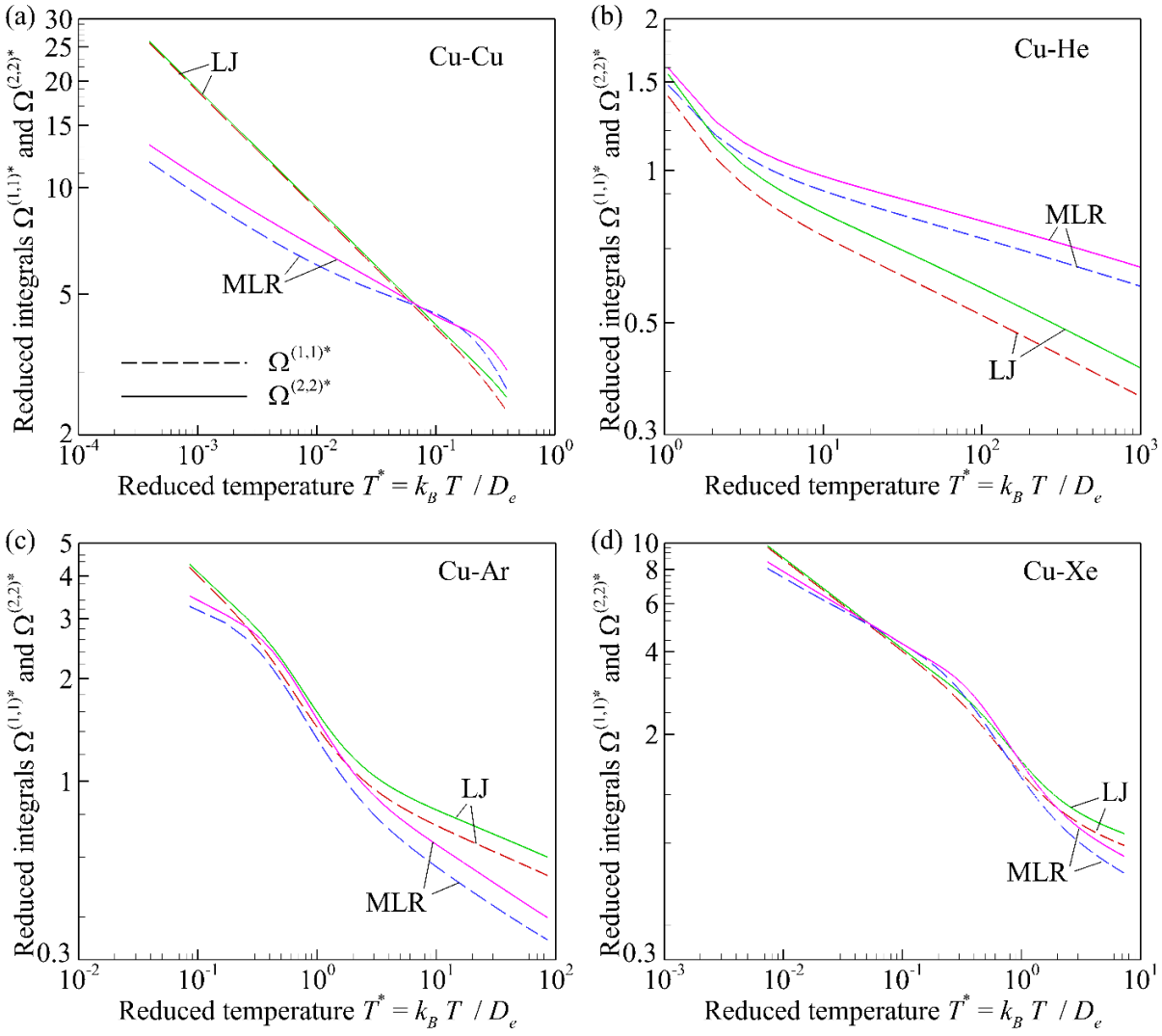

Fig. S21 Reduced integrals $\Omega^{(1.1)*}$ (dashed curves) and $\Omega^{(2.2)*}$ (solid curves) for the Cu-Cu (a), Cu-He (b), Cu-Ar (c), and Cu-Xe (c) atom pairs *versus* reduced temperature $T^* = k_B T/D_e$ calculated based on the LJ (red and green curves) and MLR (blue and magenta curves) potentials. The scale $\sigma = r_e/\sqrt[6]{2}$ is used in eqn (29).

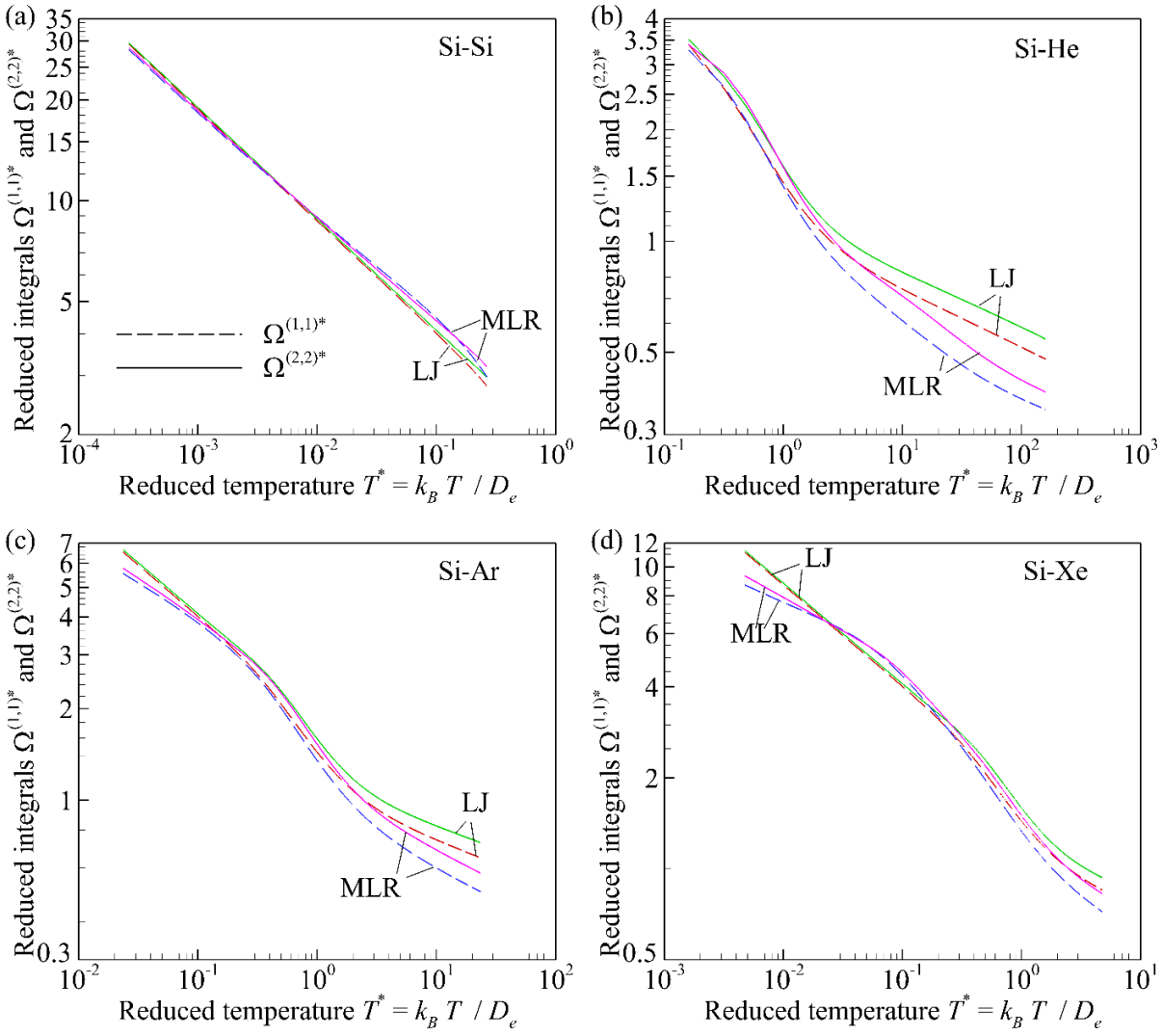

Fig. S22 Reduced integrals $\Omega^{(1.1)*}$ (dashed curves) and $\Omega^{(2.2)*}$ (solid curves) for the Si-Si (a), Si-He (b), Si-Ar (c), and Si-Xe (c) atom pairs *versus* reduced temperature $T^* = k_B T/D_e$ calculated based on the LJ (red and green curves) and MLR (blue and magenta curves) potentials. The scale $\sigma = r_e/\sqrt[6]{2}$ is used in eqn (29).

The viscosities of helium, argon, and xenon are shown in Fig. S23, where the calculations are performed based on the MLR and LJ potentials with the parameters obtained in the present work (Table 3) as well as potential functions proposed in ref. S3-S6 and S15.

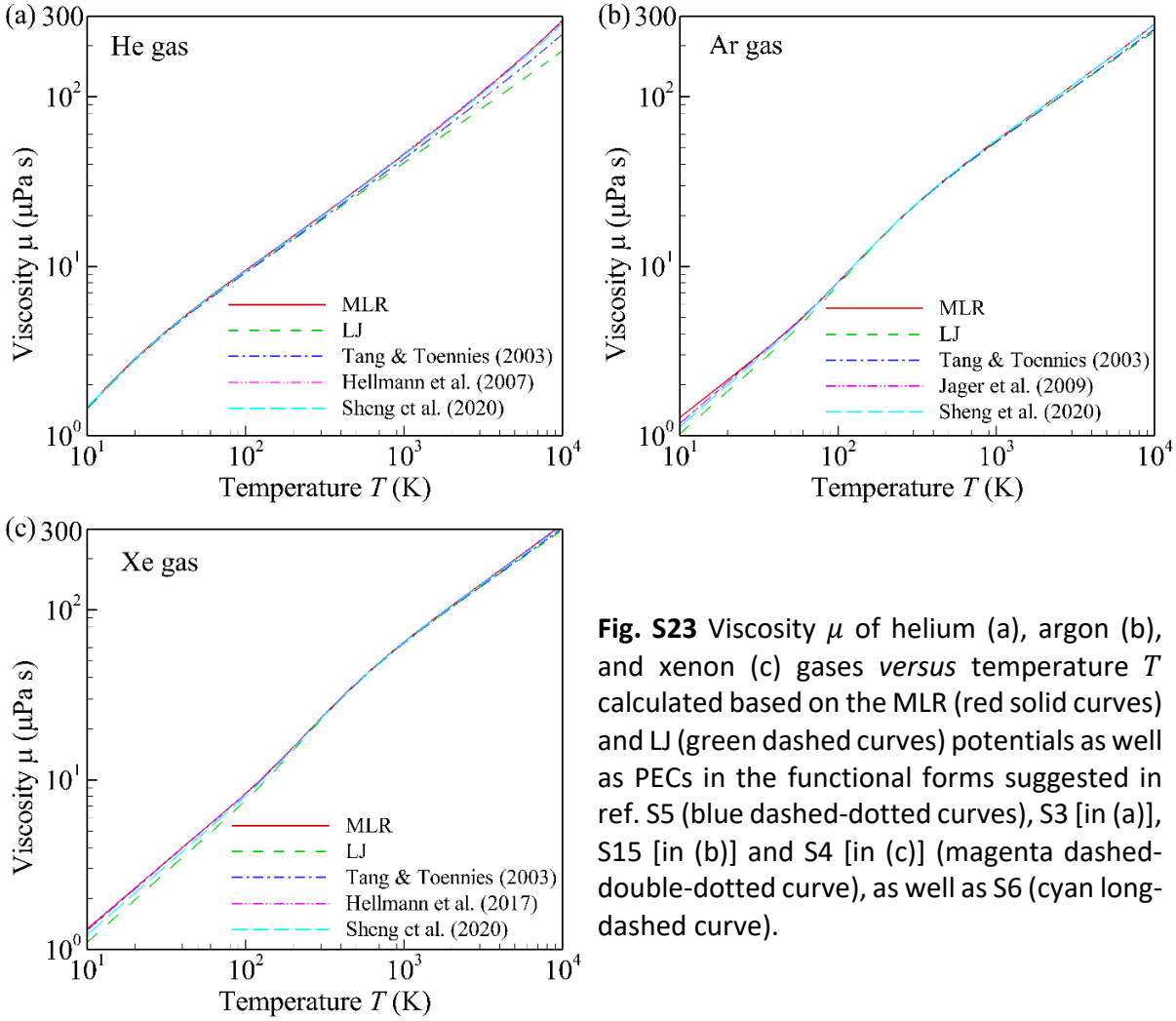

Fig. S23 Viscosity μ of helium (a), argon (b), and xenon (c) gases *versus* temperature T calculated based on the MLR (red solid curves) and LJ (green dashed curves) potentials as well as PECs in the functional forms suggested in ref. S5 (blue dashed-dotted curves), S3 [in (a)], S15 [in (b)] and S4 [in (c)] (magenta dashed-double-dotted curve), as well as S6 (cyan long-dashed curve).

In agreement with the previous analysis of the Ω-integrals, the dependences of viscosity on temperature can include three characteristic temperature ranges, where $\mu(T)$ can be approximated by a power function with different viscosity exponents in each of these temperature ranges. For argon and xenon, the Ω-integrals calculated based on the MLR and LJ potentials agree well at $T^*\sim1$ but strongly deviate from each other at smaller and larger reduced temperatures. Correspondingly, the viscosities of these gases predicted based on the MLR and LJ potentials

closely agree only at $T^*\sim1$. For helium, the difference in viscosities calculated based on the MLR and LJ potentials remains relatively large in the whole temperature range considered (Table 4).

The viscosity calculated based on the MLR potentials agrees well with the viscosity calculated based on the potential functions developed based on CCSD(T) calculations in ref. S3 for He (average disagreement $\Delta[\mu]_A\sim1\%$, see Table 4), ref. S15 for Ar ($\Delta[\mu]_A\sim0.3\%$), and ref. S4 for Xe ($\Delta[\mu]_A\sim0.3\%$) gases. The universal potential function for the noble gas dimers developed in ref. S6 provides the viscosity data that agree well with the MLR potential for argon ($\Delta[\mu]_A\sim0.1$ %) but demonstrate worse agreement for He and Xe gases. The viscosity values obtained based on the potentials suggested in ref. S5 strongly deviates from the data based on the MLR potential. For these potentials, the average differences $\Delta[\mu]_A$ are only twice smaller than the corresponding differences for the LJ potential (Table 4).

S8. Effect of the Lennard-Jones and VSS molecular model approximations on the transport coefficients of the copper-argon mixture

The ratios of the transport coefficients calculated based on the LJ and MLR potentials as well as the VSS molecular model and MLR potential for the Cu-Ar mixture are shown in Fig. S24 and S25, respectively. These results can be compared with the similar results obtained for the Cu-He mixture and shown in Fig. 13 and 14. Overall, the values of the transport coefficients calculated based on the LJ and VSS approximations of interatomic interactions in both the Cu-He and Cu-Ar mixtures strongly deviate from the values of transport coefficients calculated based on the MLR potentials that accurately approximate the *ab initio* PECs. The transport coefficients of the Cu-Ar mixture, when calculated based on the VSS molecular model with parameters marked by star "*" in Table 6, demonstrate the largest deviations from the MLR-based transport coefficients at low temperatures $T\sim100$ K.

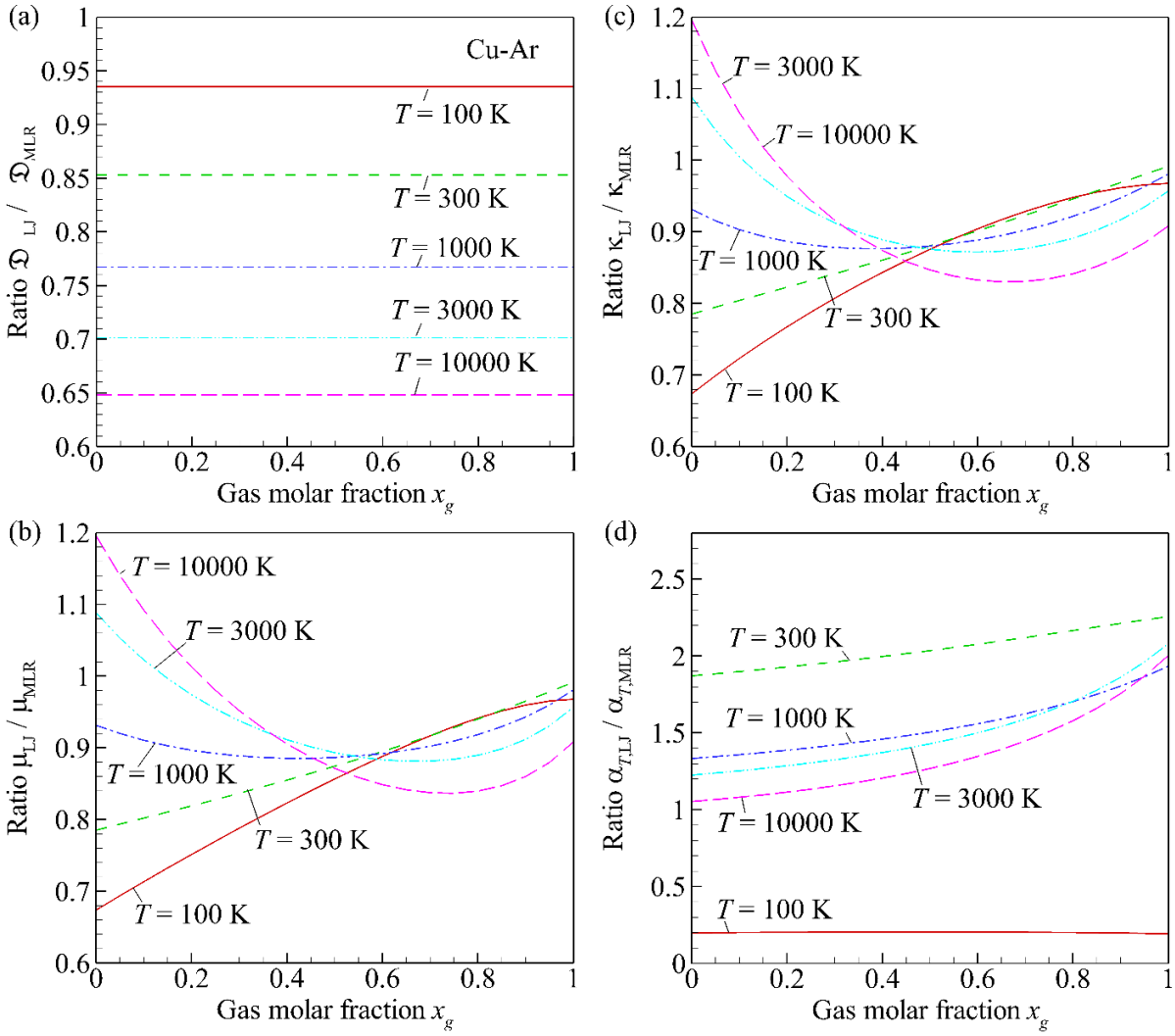

Fig. S24 Ratios of binary diffusivities $\mathfrak{D}_{\mathrm{LJ}}/\mathfrak{D}_{\mathrm{MLR}}$ (a), viscosities $\mu_{\mathrm{LJ}}/\mu_{\mathrm{MLR}}$ (b), thermal conductivities $\kappa_{\mathrm{LJ}}/\kappa_{\mathrm{MLR}}$ (c), and thermal diffusion factors $\alpha_{T,\mathrm{LJ}}/\alpha_{T,\mathrm{MLR}}$ (d) calculated based on the LJ (subscripts "LJ") and MLR (subscripts "MLR") potentials for the Cu-Ar mixture *versus* gas molar fraction x_g at a temperature of $T = 100$ K (red solid curves), 300 K (green dashed curves), 1000 K (blue dashed-dotted curves), 3000 K (cyan dashed-double-dotted curves), and 10000 K (magenta long-dashed curved). All transport coefficients are calculated based on the one-term expansions with respect to the Sonine polynomials.

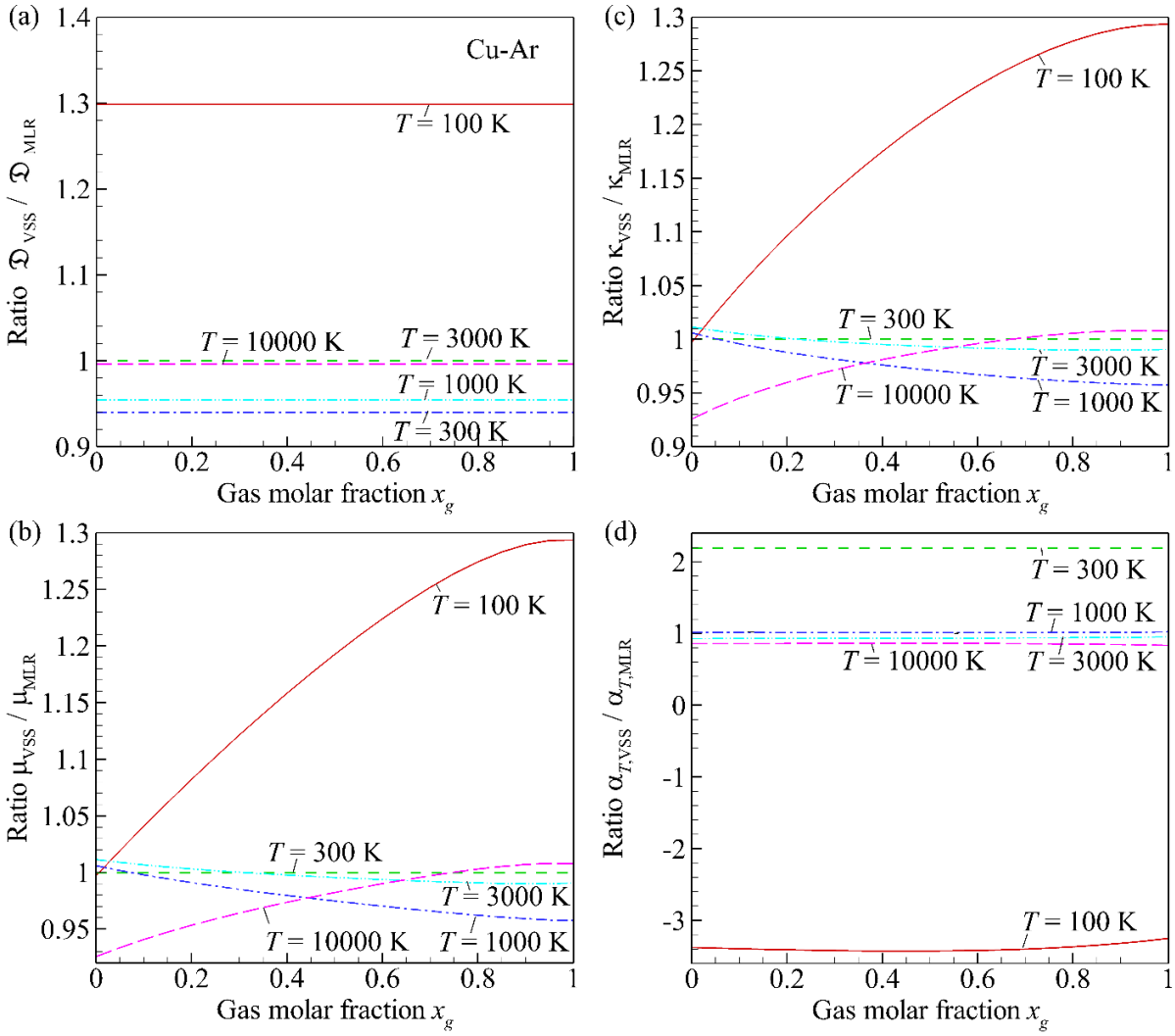

Fig. S25 Ratios of binary diffusivities $\mathfrak{D}_{\mathrm{VSS}}/\mathfrak{D}_{\mathrm{MLR}}$ (a), viscosities $\mu_{\mathrm{VSS}}/\mu_{\mathrm{MLR}}$ (b), thermal conductivities $\kappa_{\mathrm{VSS}}/\kappa_{\mathrm{MLR}}$ (c), and thermal diffusion factors $\alpha_{T,\mathrm{VSS}}/\alpha_{T,\mathrm{MLR}}$ (d) calculated based on the VSS molecular model with the parameterizations marked with "*" in Table 6 (subscripts "VSS") and MLR potential (subscripts "MLR") for the Cu-Ar mixture *versus* gas molar fraction x_g at a temperature of $T = 100$ K (red solid curves), 300 K (green dashed curves), 1000 K (blue dashed-dotted curves), 3000 K (cyan dashed-double-dotted curves), and 10000 K (magenta long-dashed curved). All transport coefficients are calculated based on the one-term expansions with respect to the Sonine polynomials.

S9. Tabulated transport coefficients

The calculated values of the transport coefficients are provided in the form of individual ASCII files, which are included into the supplementary material for this paper. In these files, all values are obtained based on the ten-term approximations of the transport coefficients with respect to the Sonine polynomials of the Chapman-Enskog theory.[S17]

For pure Cu and Si vapors, the values of self-diffusivity $\mathfrak{D}$ (mm^2 s^{-1}), viscosity μ (μPa s), and thermal conductivity κ (mW m^{-1} K^{-1}) as functions of temperature T (K) can be found in the files

Kayang_et_al_[VAP]_vapor_Diff_Visc_Cond.dat,

where [VAP] is either "Cu" or "Si". The values of the transport coefficients are calculated in the temperature range from 10^2 K to 10^4 K. The values of self-diffusivity are calculated at a pressure of 1 atm = 101325 Pa.

For binary mixtures, the values of binary diffusivity $\mathfrak{D}$ (mm^2 s^{-1}), viscosity μ (μPa s), thermal conductivity κ (mW m^{-1} K^{-1}), and thermal diffusion factor α_T as functions of temperature T (K) and molar fraction x_g of a noble gas can be found in the form of two-dimensional tables in the individual files

Kayang_et_al_[VAP]_[GAS]_[PARAM].dat,

where [VAP] is either "Cu" or "Si", [GAS] is "He", "Ar", or "Xe", and [PARAM] is "Diff" for diffusivity, "Visc" for viscosity, "Cond" for thermal conductivity, and "TDF" for thermal diffusion factor. In these files, the first line of data contains the values of molar fraction x_g. The following lines start from the temperature value. The following values are the values of the corresponding coefficient at this temperature at various x_g. In this way, the first column contains the values of temperature, and each other column starts from the value of the molar fraction and contains the values of the transport coefficient at this molar fraction at various temperatures. The values of the transport coefficients are calculated in the temperature range from 10^2 K to 10^4 K with the increment of the gas molar fraction equal to 0.05. The values of binary diffusivity are calculated at a pressure of 1 atm.

References

S1 J. Toulouse and C. J. Umrigar, Full optimization of Jastrow–Slater wave functions with application to the first-row atoms and homonuclear diatomic molecules, *J. Chem. Phys.* 2008, **128**(17), 174101.

S2 J. Kim, A. D. Baczewski, T. D. Beaudet, A. Benali, M. C. Bennett, M. A. Berrill, N. S. Blunt, E. J. L. Borda, M. Casula, D. M. Ceperley and S. Chiesa, QMCPACK: an open source ab initio quantum Monte Carlo package for the electronic structure of atoms, molecules and solids, *J. Phys. Condens. Matter*, 2018, **30**(19), 195901.

S3 R. Hellmann, E. Bich and E. Vogel, Ab initio potential energy curve for the helium atom pair and thermophysical properties of dilute helium gas. I. Helium–helium interatomic potential, *Mol. Phys.*, 2007, **105**(23-24), 3013-3023.

S4 R. Hellmann, B. Jäger and E. Bich, State-of-the-art ab initio potential energy curve for the xenon atom pair and related spectroscopic and thermophysical properties, *J. Chem. Phys.*, 2017, **147**, 034304.

S5 K. T. Tang, and J. P. Toennies, The van der Waals potentials between all the rare gas atoms from He to Rn, *J. Chem. Phys.*, 2003, **118**(11), 4976-4983.

S6 X. Sheng, J. P. Toennies and K. T. Tang, Conformal analytical potential for all the rare gas dimers over the full range of internuclear distances, *Phys. Rev. Lett.*, 2020, **125**, 253402.

S7 V. A. Petrov, O. A. Ranjbar, P. A. Zhilyaev and A. N. Volkov, Kinetic simulations of laser-induced plume expansion from a copper target into a vacuum or argon background gas based on ab initio calculation of Cu–Cu, Ar–Ar, and Ar–Cu interactions, *Phys. Fluids*, 2020, **32**(10), 102010.

S8 A. W. Hauser, A. Volk, P. Thaler and W. E. Ernst, Atomic collisions in suprafluid helium-nanodroplets: timescales for metal-cluster formation derived from He-density functional theory, *Phys. Chem. Chem. Phys.*, 2015, **17**(16), 10805-10812.

S9 F. Cargnoni, T. Kuś, M. Mella and R. J. Bartlett, Ground state potential energy surfaces and bound states of M–He dimers (M = Cu, Ag, Au): a theoretical investigation, *J. Chem. Phys.*, 2008, **129**(20), 204307.

S10 X. F. Tong, C. L. Yang, Y. P. An, M. S. Wang, X. G. Ma and D. H. Wang, Theoretical characteristics of the bound states of MX complexes (M = Cu, Ag, and Au, and X = He, Ne, and Ar), *J. Chem. Phys.*, 2009, **131**(24), 244304.

S11 D. A. Dixon, D. Feller, K. A. Peterson and J. L. Gole, The molecular structure and ionization potential of Si2: the role of the excited states in the photoionization of Si_2, *J. Phys. Chem. A*, 2000, **104**(11), 2326-2332.

S12 C. Tao, A. Teslja, P. J. Dagdigian, S. Atahan and M. H. Alexander, Laser spectroscopic study of the SiAr van der Waals complex, *J. Chem. Phys.*, 2002, **116**(21), 9239-9248.

S13 G. A. Bird, Monte Carlo simulation in an engineering context, *Progr. Astro. Aero.*, 1981, **74**(1), 239-255.

S14 K. Koura and H. Matsumoto, Variable soft sphere molecular model for inverse-power-law or Lennard-Jones potential, *Phys. Fluids A: Fluid Dyn.*, 1991, **3**, 2459-2465.

S15 B. Jäger, R. Hellmann, E. Bich and E. Vogel, Ab initio pair potential energy curve for the argon atom pair and thermophysical properties of the dilute argon gas. I. Argon–argon interatomic potential and rovibrational spectra, *Mol. Phys.*, 2009, **107**(20) 2181-2188 [correction in Vol.108, 105 (2010)].

S16 F. Sharipov and G. Bertoldo, Numerical solution of the linearized Boltzmann equation for an arbitrary intermolecular potential, *J. Comp. Phys.*, 2009, **228**(9), 3345-3357.

S17 F. Sharipov and V. J. Benites, Transport coefficients of helium-argon mixture based on ab initio potential,*J. Chem. Phys.*, 2015, **143**, 154104.